European Journal of Medicinal Chemistry 130 (2017) 124–138

Contents lists available at ScienceDirect

European Journal of Medicinal Chemistry

journal homepage: http://www.elsevier.com/locate/ejmech

Research paper

New azole derivatives showing antimicrobial effects and their mechanism of antifungal activity by molecular modeling studies

İnci Selin Doğan [a, 1], Selma Saraç [a, *], Suat Sari [a], Didem Kart [b], Şebnem Eşsiz Gökhan [c], İmran Vural [d], Sevim Dalkara [a]

[a] Department of Pharmaceutical Chemistry, Hacettepe University, Faculty of Pharmacy, 06100, Ankara, Turkey
[b] Department of Pharmaceutical Microbiology, Hacettepe University, Faculty of Pharmacy, 06100, Ankara, Turkey
[c] Department of Bioinformatics and Genetics, Kadir Has University, Faculty of Engineering and Natural Sciences, 34083, Istanbul, Turkey
[d] Department of Pharmaceutical Technology, Hacettepe University, Faculty of Pharmacy, 06100, Ankara, Turkey

ARTICLE INFO

Article history:
Received 8 December 2016
Received in revised form
20 January 2017
Accepted 13 February 2017
Available online 17 February 2017

Keywords:
Azoles
Antifungal
Candida species
CYP51
Molecular docking
Molecular dynamics simulation

ABSTRACT

Azole antifungals are potent inhibitors of fungal lanosterol 14α demethylase (CYP51) and have been used for eradication of systemic candidiasis clinically. Herein we report the design, synthesis, and biological evaluation of a series of 1-phenyl/1-(4-chlorophenyl)-2-(1*H*-imidazol-1-yl)ethanol esters. Many of these derivatives showed fungal growth inhibition at very low concentrations. Minimal inhibition concentration (MIC) value of **15** was 0.125 μg/mL against *Candida albicans*. Additionally, some of our compounds, such as **19** (MIC: 0.25 μg/mL), were potent against resistant *C. glabrata*, a fungal strain less susceptible to some first-line antifungal drugs. We confirmed their antifungal efficacy by antibiofilm test and their safety against human monocytes by cytotoxicity assay. To rationalize their mechanism of action, we performed computational analysis utilizing molecular docking and dynamics simulations on the *C. albicans* and *C. glabrata* CYP51 (CACYP51 and CGCYP51) homology models we built. Leu130 and T131 emerged as possible key residues for inhibition of CGCYP51 by **19**.

1. Introduction

Systemic candidiasis is the 4th most prevalent hospital-acquired systemic infection, especially common among immunocompromised patients since it is opportunistic, and associated with severe mortality [1–4]. *Candida albicans* is the major pathogen identified in most of the cases, however infections caused by non-albicans *Candida* (nAC), have been reported to emerge with increasing mortality and resistance to first-line antifungals [5–7]. Especially, some *C. glabrata* strains are known to be intrinsically less susceptible to echinocandins and azole antifungals although they lack certain virulence factors that *C. albicans* has [8].

Azole antifungals are widely used for the treatment of fungal infections. They inhibit lanosterol 14α demethylase (CYP51), a monooxygenase in fungal cells, which results in depletion of ergosterol, a major component of fungal cell membrane [9]. Azole antifungals compete with the natural ligand lanosterol and form a strong coordination with the iron of heme present in the catalytic site of CYP51 via the N in their azole moieties replacing O_2 [10]. One of the mechanisms proposed for the resistance of *C. glabrata* against azoles is low affinity of their CYP51 to these agents as observed in some *C. albicans* strains [11,12]. Therefore new agents effective against resistant strains are needed for antifungal chemotherapy.

Biofilms are known as microbial communities irreversibly attached to a surface and encapsulated in a self-produced polymeric matrix. Resistance to antimicrobial treatment is one of their major characteristics [13]. Many azole antifungals were found inactive against biofilm forming pathogens. It is anticipated that compounds with antibiofilm activities may decrease the production of virulence factors by microorganisms and their tolerance to drugs at lower doses. This leads to the reduction of pathogenicity of microorganism without killing it so that eradication of resistance development could be achieved [14].

We previously reported some 1-(2-naphthyl)-2-(1*H*-imidazol-1-yl)ethanone oxime ether and 1-(2-naphthyl)-2-(imidazole-1-yl) ethanol ester derivatives with moderate to potent antifungal activities [15,16]. The common naphthalene pharmacophore of these

* Corresponding author.
E-mail address: sesarac@hacettepe.edu.tr (S. Saraç).
[1] Permanent address: Department of Pharmaceutical Chemistry, Karadeniz Technical University, Faculty of Pharmacy, 61080, Trabzon, Turkey.

http://dx.doi.org/10.1016/j.ejmech.2017.02.035
0223-5234/

derivatives, was suggested to decrease antifungal efficacy by De Vita et al., who reported several potent antifungals in 1-phenyl-2-(imidazole-1-yl)ethyl carbamate scaffold [17,18]. Herein we present a series of 1-phenyl/1-(4-chlorophenyl)-2-(1*H*-imidazol-1-yl) ethanol esters with strong inhibitory activities against some standard fungi strains including *C. albicans* and clinically resistant *C. glabrata*, moderate inhibitory activity against standard Gr (+) and Gr (-) bacteria by broth microdilution and antibiofilm tests along with their cytotoxicity screenings. In addition to these, we report homology modeling of *C. albicans* CYP51 (CACYP51) using a high sequence identity template. We utilized comparative modeling techniques for building the missing loop in the crystal structure of *C. glabrata* (CGCYP51) as well. We performed molecular docking and molecular dynamics (MD) simulations using these homology models in order to get further mechanistic insights into their inhibition of both CYP51 enzymes in a comparative manner.

The molecular design of the compounds was based on azole antifungals which principally consist of 4 pharmacophores: an iron coordinating azole ring (A) to coordinate heme iron, an aromatic ring (B) usually phenyl or halogeno-substituted phenyl ring which is connected to A by an alkyl bridge of 2 C length, an aromatic ring on this alkyl bridge (C), and additional lipophilic groups connected to C (D), the last two of which together are usually referred to as "tail" [17,25] (Fig. 1). In order to evaluate the necessity of aromaticity in the tail group for the activity, we included aliphatic groups such as straight chain (**1-4**, **7**, **16-19, 22**), branched-chain (**5**, **6**, **20**, **21**), unsaturated aliphatic (**8**, **23**), and cycloaliphatic (**13**, **28**); as well as arylalkyl (**9-11**, **24-26**), α,β-unsaturated aromatic (**12**, **27**), and aromatic (**14**, **15**, **29**, **30**) moieties as part of the tail. In this manner we sought to establish new structure-activity relationships (SARs) regarding the type and the size of the R_2 group. Since most of the azole antifungals contain halogeno-substituted aromatic group,

2. Results and discussion

2.1. Chemistry

As shown in Scheme 1, we synthesized the final compounds (**1-30**) by the reaction of 1-phenyl/1-(4-chlorophenyl)-2-(1*H*-imidazol-1-yl)ethanols (**g** and **h**) with various carboxylic acids according to Steglich esterification reaction [19–22] using dicyclohexylcarbodiimide (DCC) as a coupling reagent and 4-dimethylaminopyridine (DMAP) as a hypernucleophilic acylation catalyst under mild conditions in moderate yields. The ethanol derivatives were obtained through reduction of their ketone precursors (**e** and **f**) and the ketones by N-alkylation of 1*H*-imidazole with 2-bromoacetophenone (**c**) and 2-bromo-4-chloroacetophenone (**d**). We prepared **c** and **d** by brominating **a** and **b**. The final compounds were prepared as hydrochloride salts to increase their solubility especially for *in vitro* broth microdilution tests. Among the ester derivatives **1**, **15**, and **30** were previously reported [17,23,24]; others are reported for the first time in this study.

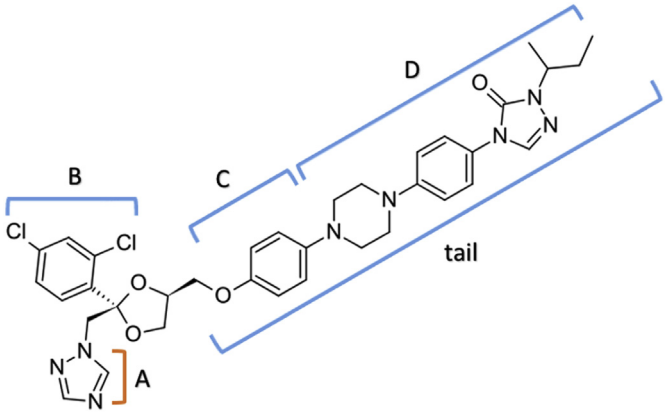

Fig. 1. (single column). Common pharmacophores in azole antifungals represented on itraconazole: a heme-coordinating group (A), a phenyl or halogenated phenyl ring (B), an aromatic ring (C), and additional lipophilic groups (D). C and D together are referred to as "tail".

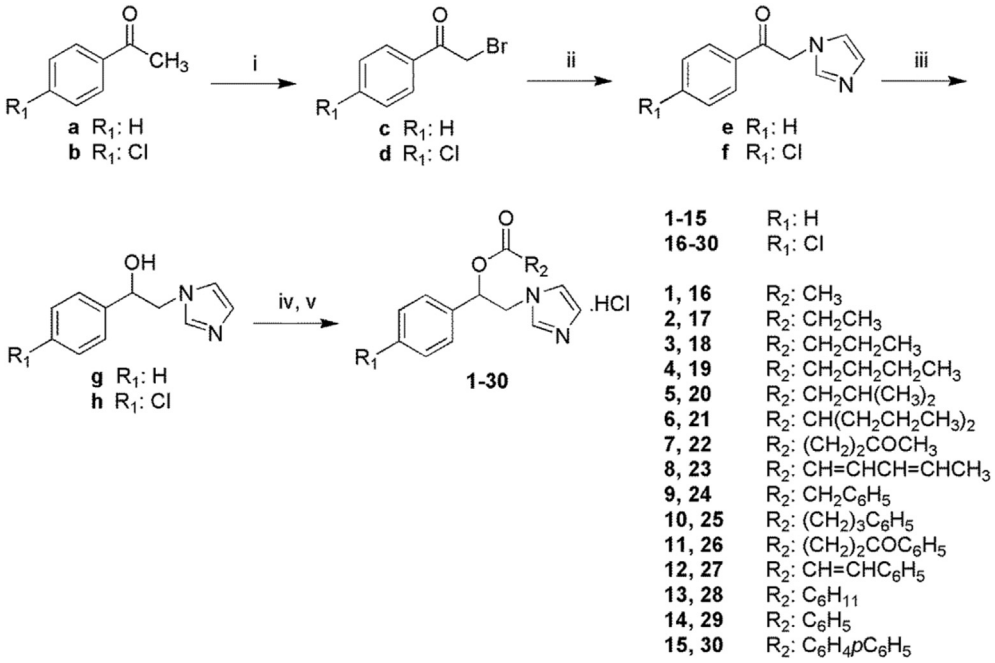

Scheme 1. (double column). Reagents and conditions: (i) CH_3COOH, HBr, Br_2, 0 °C to rt; (ii) 1*H*-imidazole, DMF, 0 °C to rt; (iii) CH_3OH, $NaBH_4$, 0–5 °C; (iv) DCC, DMAP, DCM, R_2-COOH, 0 °C to rt; (v) Diethyl ether, gHCl.

we included 4-chlorophenyl ring along with phenyl ring as pharmacophore B.

2.2. Biological activity

2.2.1. Antifungal activity

According to the MIC values of **1**–**30** and the reference drug (fluconazole) against standard *Candida* strains (Table 1) a chlorine atom at the 4th position of the phenylethyl moiety generally resulted in increased antifungal activity except valproic (**6**), cinnamic (**12**) and 4-biphenylcarboxylic acid (**15**) esters of 1-phenyl-2-ethanol, which revealed lower MIC values than their corresponding 1-(4-chlorophenyl)-2-ethanol esters (**21**, **27**, **30**). However, De Vita and co-workers [17] concluded that the presence of a halogen atom at the 4th position of phenylethyl moiety did not markedly affect the antifungal activity of some carbamic acid and 4-biphenylcarboxylic acid ester derivatives. In this context it should be pointed out that the antifungal activity results of **15** and **30**, 4-biphenylcarboxylic acid ester derivatives, were in accordance with their previously published results by De Vita and co-workers [17].

In general **15** and **30**, which have an additional aromatic group (D) in the tail, were the most potent derivatives. However some other derivatives (**5**, **18**, **19**, **20**, **23**, and **28**) among the series also proved promising. Especially **20**, with only an isopentyl group for the tail showed comparably good MIC values against *C. albicans* and nAC species regarding fluconazole. Therefore, we conclude that aromaticity for C and D is important but not essential for good antifungal activity. Additionally lengthening, branching, unsaturation and cyclization of the alkyl chain in the ester group had no significant effect on the antifungal activity.

Table 1
MIC values (μg/mL) of **1**–**30**, **g**, **h**, and fluconazole against standard fungal strains.

Compound	*C. albicans* ATCC 90028	*C. krusei* ATCC 6258	*C. parapsilosis* ATCC 90018
1	128	128	64
2	64	32	8
3	64	32	16
4	8	32	8
5	2	32	2
6	32	32	32
7	256	256	256
8	32	32	8
9	64	128	32
10	4	32	4
11	16	128	32
12	1	16	1
13	16	128	16
14	32	64	32
15	0.125	8	0.125
16	64	32	8
17	4	32	4
18	0.5	4	1
19	0.5	8	0.5
20	0.25	4	0.25
21	128	64	64
22	64	32	16
23	0.5	8	1
24	0.5	4	2
25	2	8	2
26	4	16	4
27	4	16	2
28	1	8	1
29	4	32	2
30	0.25	4	0.25
g	256	256	256
h	128	256	128
Fluconazole	0.25	16	0.25

Against *C. albicans* **20** and **30** were equally potent as fluconazole (MIC 0.25 μg/mL) while **15** was the most active with even a lower MIC value (MIC 0.125 μg/mL). Many compounds were either equally active (**12**, **26,** and **27**) as or more active (**15**, **18**, **19**, **20**, **23-25**, and **30**) than fluconazole against *C. krusei*, which is intrinsically less sensitive to fluconazole [26]. Thus, we speculate that *C. krusei* probably has less intrinsic resistance to some of our compounds than certain azole antifungals such as itraconazole and voriconazole, if not at all [27]. We observed a similar trend in the potency of our compounds against *C. parapsilosis*, a rather susceptible strain to fluconazole, as **15** (MIC 0.125 μg/mL), **20**, and **30** (MIC 0.25 μg/mL) proved the most active derivatives. In addition, some of our compounds (**12**, **18**, **19**, **23**, and **28**) showed comparable MIC values (0.5–1 μg/mL) to fluconazole.

The antifungal activity of this group of compounds are enantioselective against *C. albicans* according to the data of De Vita et al. [17,18], who separated and screened the enantiomers of **15** and found that the (-) isomer was much more active than (+) isomer.

Some *C. glabrata* strains are among the nACs resistant to first-line antifungal drugs including fluconazole. Therefore, the derivatives which previously proved promising against standard *Candida* strains were evaluated against clinically resistant isolate of *C. glabrata* (Table 2) using the same broth microdilution method. Most of the selected compounds (**12**, **15**, **18-20**, **23-25**, and **27-30**) were more active than fluconazole with MICs in the range of 0.25–16 μg/mL. Among them **19** and **28** stood out with MIC values (0.25 and 0.5 μg/mL, respectively) lower than **15** and **30** (MIC 2 and 4 μg/mL, respectively), and much lower than fluconazole (MIC 32 μg/mL). In the case of clinically resistant *C. glabrata*, the derivatives with an aliphatic moiety as the tail group apparently outperformed those with aromatic moiety/moieties instead and the 4-chloro substitution to the phenyl ring on pharmacophore B dramatically boosted their efficacy.

Esterification is a widely used strategy to prepare prodrug. Therefore we attempted to evaluate antifungal activity of **g** and **h** as well to test the idea whether they act as prodrug. Since their MIC values were much higher than most of the ester derivatives this hypothesis was disproved.

Some *Candida* species are less susceptible to antifungal agents because of the resistance via biofilm formation during the prolonged therapy of clinical infections [28]. For this reason, development of new derivatives with anti-biofilm activity is an important issue for the treatment of persistent infections [29]. For this reason the anti-biofilm activity of **12**, **15**, **18-20**, **28**, and **30** was investigated against *C. albicans* (SC5314). According to the data expressed as minimal biofilm eradication concentration (MBEC) and minimal biofilm inhibition concentration (MBIC) values (Table 3), the derivatives were good at biofilm inhibition except **18** but they required relatively high concentrations for biofilm eradication.

Table 2
MIC values (μg/mL) of some of the ester derivatives and fluconazole against clinically resistant *C. glabrata*.

Compound	MIC	Compound	MIC
4	32	**20**	1
5	>32	**23**	4
6	>32	**24**	4
10	>32	**25**	8
12	8	**26**	32
14	>32	**27**	2
15	2	**28**	0.5
17	32	**29**	16
18	16	**30**	4
19	0.25	**Fluconazole**	32

Table 3
MBEC and MBIC values (μg/mL) of some of the ester derivatives against *C. albicans* (SC5314).

Compound	MBEC	MBIC
12	1024	8
15	1024	8
18	1024	>32
19	1024	8
20	1024	8
23	1024	8
28	512	8
30	512	4

2.2.2. Antibacterial activity

The antibacterial activity results indicate that all compounds were more effective against the Gram (+) bacteria than the Gram(-) bacteria (Table 4). Among the series **10**, **12**, and **26** showed the best MIC value (8 μg/mL) against *S. aureus* while **6**, **13,** and **21** against *E. faecalis*. Still these derivatives were far from comparable to the reference antibacterial drug, ciprofloxacin in terms of efficacy.

2.2.3. In vitro cytotoxic activity

Since the selectivity of the compounds is important for being a good drug candidate, the *in vitro* toxicity of the selected active compounds (**12**, **15**, **17-20**, and **23-30**) were estimated by analyzing the dose-related effects towards the growth of cultured human monocytic cell line (U937). The preliminary results showed an average 70–80% cell viability in the presence of each compound at concentrations ranging from 10-100 μg/mL. These findings indicate that the tested compounds are safe at therapeutic concentrations towards human monocytic cells.

Table 4
MIC values (μg/mL) of **1**–**30**, **g**, **h**, and ciprofloxacin against standard bacterial strains.

Compound	*S. aureus* ATCC 29213	*E. faecalis* ATCC 29212	*E. coli* ATCC 25922	*P. aeruginosa* ATCC 27853
1	1024	256	512	256
2	1024	128	512	256
3	512	128	512	256
4	256	128	512	256
5	256	128	512	256
6	16	32	512	256
7	512	128	512	256
8	512	64	512	256
9	128	64	512	128
10	8	128	1024	256
11	128	64	512	256
12	8	64	512	256
13	64	32	512	256
14	64	64	256	256
15	512	128	512	256
16	256	256	512	256
17	256	256	512	256
18	64	256	512	256
19	32	128	512	256
20	32	128	512	256
21	1024	32	512	256
22	512	256	512	256
23	16	128	512	256
24	16	256	256	256
25	128	128	512	512
26	8	256	256	256
27	1024	256	512	256
28	256	512	256	1024
29	128	512	512	256
30	512	256	512	256
g	1024	512	512	512
h	64	128	256	256
Ciprofloxacin	0.5	1.5	0.005	1.5

2.3. Molecular modeling studies

2.3.1. Homology modeling of CACYP51 and its equilibration

A BLAST [30] search among protein data bank proteins for the CACYP51 sequence yielded the CYP51 of *Saccharomyces cerevisiae* (PDB id: 5EQB [31]) as the highest-identity template (65%) available. The pairwise alignment of these sequences showed high conservation especially for the residues lining the active site gorge (Fig. 2). Superposition of Cα atoms of the template and the homology model gave a 7.00 Å RMSD value. According to the structural analysis results obtained from PROCHECK [32] 99.5% of all the residues were in favored or allowed regions of the Ramachandran plot, 98.5% of bond lengths, 92.2% of bond angles, and all planar groups were within limits (Fig. 3). These findings together showed that the raw homology model created by MODELLER [33] is satisfactory. Eukaryotic CYP51 enzymes are usually found anchored to cytoplasmic reticulum membrane, for this reason we submitted the model to PPM server [34] in order to identify the membrane-bound residues and the results were mainly in accordance with those of 5EQB reported previously [31]. Prior to docking experiments we equilibrated the itraconazole-bound model in a water box during a 1-ns MD simulations run. The RMSD of the Cα atoms stabilized to ~1.7 Å regarding the initial protein conformation at around 400 ps (Fig. 4**A**). The total energy of the system reached −1.68 kcal/mol upon heating to 310 K and was steady throughout the run (Fig. 4**B**). The RMS fluctuations plot (Fig. 4**C**) of the residues show that the outermost solvent accessible loops were the most mobile while the conserved residues which include the binding site were relatively stable.

2.3.2. CACYP51 docking

At the end of the MD simulations of CACYP51 we extracted the protein from the final frame and following its preparation we were able to re-docked itraconazole in its active site successfully (RMSD 0.86 Å). We docked some of our active compounds along with fluconazole, using this equilibrated homology model. Eukaryotic CYP enzymes share a lipophilic active site buried deep and contains an iron-containing heme co-factor [35]. The binding modes of the docked ligands showed good fit in the catalytic site similar to the co-crystallized itraconazole and followed a common trend known for the azole antifungals co-crystallized with CYP enzymes: The N3 of the imidazole ring (A) made a coordination with the Fe^{+2} of heme, the phenyl/4-chlorophenyl ring (A) positioned between I131 and F126, and the tail group (C and D) stretched along the gorge which leads up to the entrance of the catalytic site (Fig. 5). **15** and **30**, with their long, lipophilic 4-biphenyl tail, were able to partly fill this gorge and provide hydrophobic interactions such as π-π stacks with Y118 and F380 aromatic side chains. Mutation of the latter was reported to result in fluconazole resistance [36]. Fluconazole, which has a triazole ring as tail, was less effective at these interactions, however itraconazole with a much longer tail was able to fully fill the active site gorge up to the mouth. Indeed, strong binding affinity of itraconazole to CACYP51 regarding fluconazole was previously reported in several enzyme binding studies [37,38]. The relatively higher potency observed with the compounds with 4-chlorophenyl than those with phenyl (B) instead could be explained by the ability of the 4-Cl to better occupy the cleft between I131 and G303 to make additional Van der Waals contacts (Fig. 5).

2.3.3. CGCYP51 docking

The biological activity results of our compounds for *C. albicans* and *C. glabrata* revealed a reverse trend among the compounds,

```
CACYP51  4    VETVIDGINYFLSLSVTQQISILLGVPFVYNLVWQYLYSLRKDRAPLVFYWIPWFGSAAS  63
              +E V  G+++FL+L + Q+IS+++ +PF+YN+VWQ LYSLRKDR PLVFYWIPW GSA
5EQB     7    LEYVNIGLSHFLALPLAQRISLIIIIPFIYNIVWQLLYSLRKDRPPLVFYWIPWVGSAVV  66

CACYP51  64   YGQQPYEFFESCRQKYGDVFSFMLLGKIMTVYLGPKGHEFVFNAKLSDVSAEDAYKHLTT  123
              YG +PYEFFE C++KYGD+FSF+LLG++MTVYLGPKGHEFVFNAKL+DVSAE AY HLTT
5EQB     67   YGMKPYEFFEECQKKYGDIFSFVLLGRVMTVYLGPKGHEFVFNAKLADVSAEAAYAHLTT  126

CACYP51  124  PVFGKGVIYDCPNSRLMEQKKFAKFALTTDSFKRYVPKIREEILNYFVTDESFKLKEKTH  183
              PVFGKGVIYDCPNSRLMEQKKF K ALT ++FK YVP I EE+  YF   ++F+L E+T
5EQB     127  PVFGKGVIYDCPNSRLMEQKKFVKGALTKEAFKSYVPLIAEEVYKYFRDSKNFRLNERTT  186

CACYP51  184  GVANVMKTQPEITIFTASRSLFGDEMRRIFDRSFAQLYSDLDKGFTPINFVFPNLPLPHY  243
              G  +VM TQPE+TIFTASRSL G EMR   D  FA LYSDLDKGFTPINFVFPNLPL HY
5EQB     187  GTIDVMVTQPEMTIFTASRSLLGKEMRAKLDTDFAYLYSDLDKGFTPINFVFPNLPLEHY  246

CACYP51  244  WRRDAAQKKISATYMKEIKSRRERGDIDPNRDLIDSLLIHSTYKDGVKMTDQEIANLLIG  303
               +RD AQK IS TYM  IK RR+  DI  +RDLIDSL+ +STYKDGVKMTDQEIANLLIG
5EQB     247  RKRDHAQKAISGTYMSLIKERRKNNDIQ-DRDLIDSLMKNSTYKDGVKMTDQEIANLLIG  305

CACYP51  304  ILMGGQHTSASTSAWFLLHLGEKPHLQDVIYQEVVELLKEKGGDLNDLTYEDLQKLPSVN  363
              +LMGGQHTSA+TSAW LLHL E+P +Q  +Y+E + +L    G   +LTY+ LQ++P +N
5EQB     306  VLMGGQHTSAATSAWILLHLAERPDVQQELYEEQMRVLD---GGKKELTYDLLQEMPLLN  362

CACYP51  364  NTIKETLRMHMPLHSIFRKVTNPLRIPETNYIVPKGHYVLVSPGYAHTSERYFDNPEDFD  423
               TIKETLRMH PLHS+FRKV   + +P T+Y++P G++VLVSPGY H  + YF N   F+
5EQB     363  QTIKETLRMHHPLHSLFRKVMKDMHVPNTSYVIPAGYHVLVSPGYTHLRDEYFPNAHQFN  422

CACYP51  424  PTRWDTAAAKANSVSFNSSDEVDYGFGKVSKGVSSPYLPFGGGRHRCIGEQFAYVQLGTI  483
               RW+  +A + SV     +EVDYGFG +SKGVSSPYLPFGGGRHRCIGE FAY QLG +
5EQB     423  IHRWNNDSASSYSV----GEEVDYGFGAISKGVSSPYLPFGGGRHRCIGEHFAYCQLGVL  478

CACYP51  484  LTTFVYNLRWTI-DGYKVPDPDYSSMVVLPTEPAEIIWEKR  523
              ++ F+  L+W   +G  VP PD++SMV LPT PA+IIWEKR
5EQB     479  MSIFIRTLKWHYPEGKTVPPPDFTSMVTLPTGPAKIIWEKR  519
```

Fig. 2. (1.5 column). Pairwise alignment of query (CACYP51) and template (5EQB) sequences. Identical residues (65%) are highlighted as red letters and similar residues (78%) as red pluses (+) in each middle row. Membrane-bound residues are emphasized in yellow and binding site residues showed in green fonts. (For interpretation of the references to colour in this figure legend, the reader is referred to the web version of this article.)

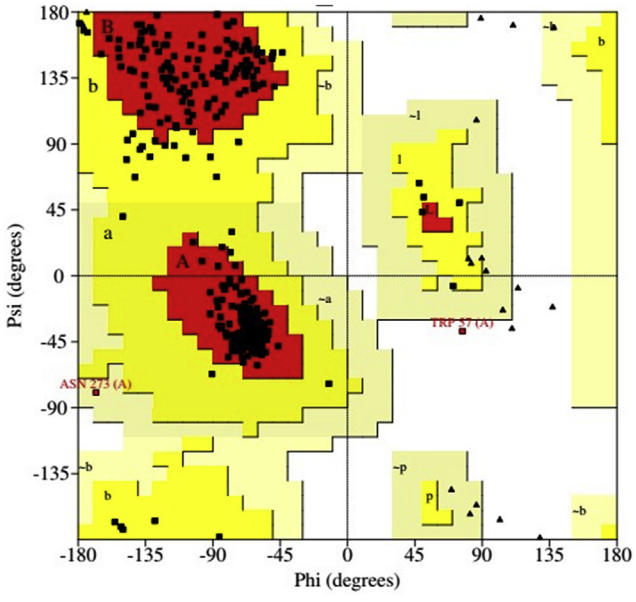

Fig. 3. (1.5 column). Ramachandran plot of the selected raw model of CACYP51. Red indicates most favored, yellow additional allowed, tan generously allowed, and white disallowed areas. 92%, 7.5%, 0.2%, and 0.2% of the residues fall into these areas, respectively. End residues (2), glycines (32), and prolines (29) are ignored. (For interpretation of the references to colour in this figure legend, the reader is referred to the web version of this article.)

such that with aromatic tail, (e.g. **15** and **30**), were less potent than those with aliphatic tail, namely **19** and **28**, against *C. glabrata*. The impact of 4-chloro substitution on the phenyl group (B) on the activity was more stressed in the case *C. glabrata*. We aimed to perform molecular docking of our compounds into the active site of the X-ray structure of CGCYP51 (PDB id: 5JLC [39]) to find the underlying reasons for these phenomena at atomic level. But before that we modeled the missing loop between residues 435-443 of the X-ray structure. This was performed by simply following the same protocol for CACYP51 using the intact CGCYP51 sequence and 5JLC as template without equilibration. With the addition of the missing residues, a long loop between residues 410-446 was formed, which, then, was optimized using MODELLER's loop refining script. We used this optimized and intact homology model for docking our active compounds followed by MD simulations. The docking poses of the compounds in CGCYP51's active site were similar to those we obtained from CACYP51 and in good consistency as expected. The aliphatic tails of **19** and **28** made hydrophobic contacts with the aliphatic groups of L130 and T131 side chains and the aromatic side chain of Y127 (Fig. 6**A-C**). In the case of **15**, however, the 4-biphenyl moiety was rather closer to Y127 to make π-π stack, which was the case with triazole tail of fluconazole, too. Thanks to the 4-chloro substituent on the phenyl ring, **19** and **28** more effectively filled the lipophilic cavity between L308 and V312 side chains (Fig. 6**D**).

In order to further test some of these suggestions we ran MD simulations of a water-solvated CGCYP51 system including the docked conformer of **19** in its binding site for 2 ns. The RMSD values of protein Cα atoms and system's total energy plots over time showed system's stability with **19**'s presence in the active site (Fig. 7). We monitored the distance between L130 side chain CD2

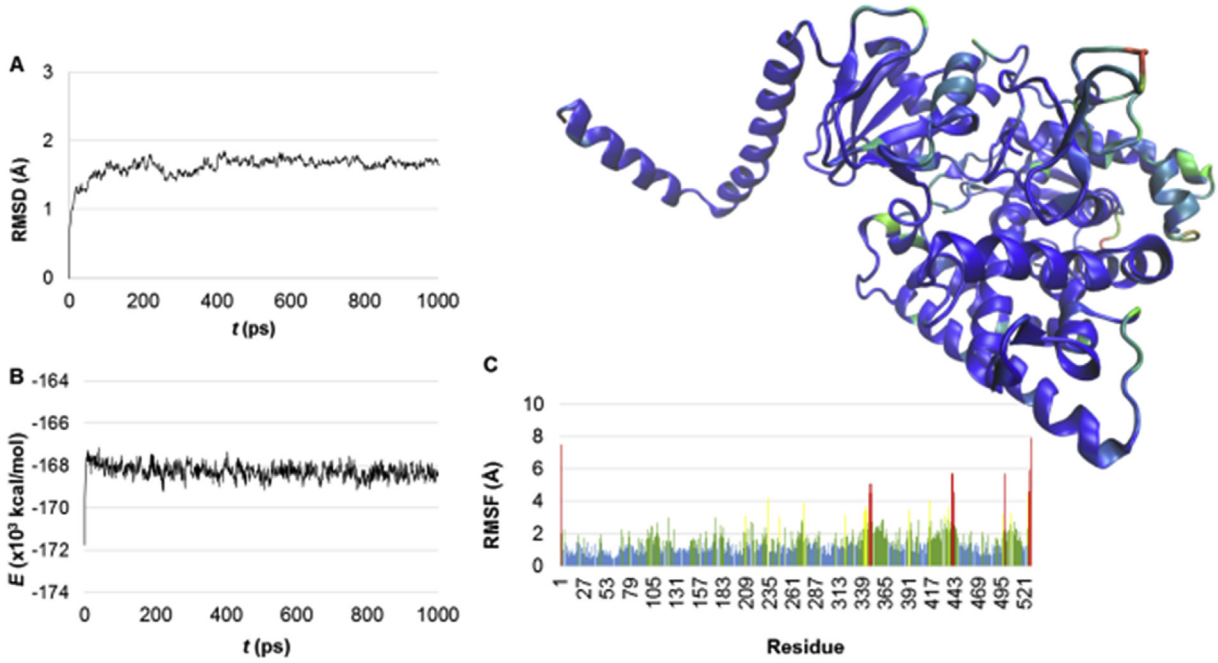

Fig. 4. (double column). Plots of itraconazole-bound CACYP51's Cα RMSD values (**A**) and protein total energy (**B**) over time and RMS fluctuations of each residue (**C**). CACYP51 in coloured ribbons according to RMSF.

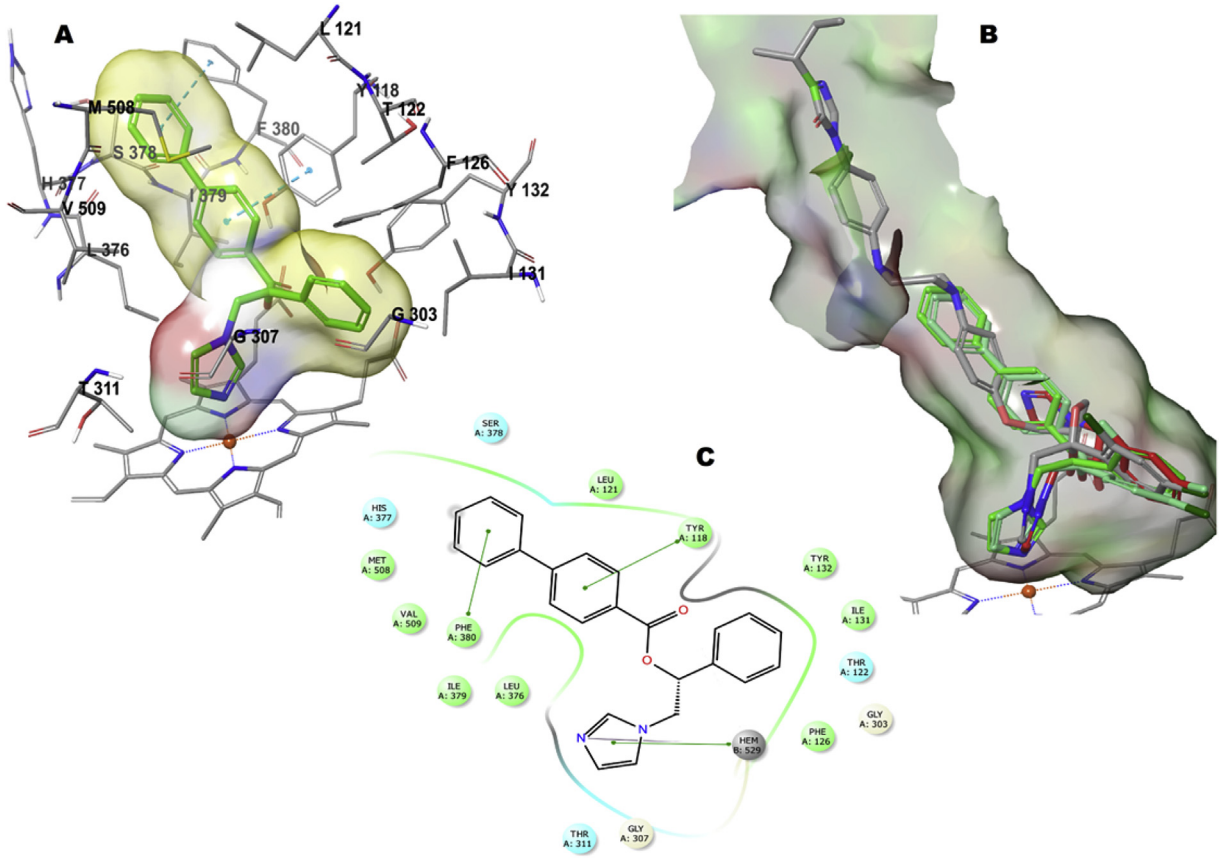

Fig. 5. (double column). Binding interactions of **15** (green sticks, surface is rendered) with the active site residues (grey sticks, Fe^{+2} as CPK) of CACYP51 (**A**); superposition of **15** (green), **30** (aquamarine), fluconazole (blue), and itraconazole (grey) in CACYP51 active site (surface is rendered) (**B**); 2-D interaction diagram of **B** (**C**). (For interpretation of the references to colour in this figure legend, the reader is referred to the web version of this article.)

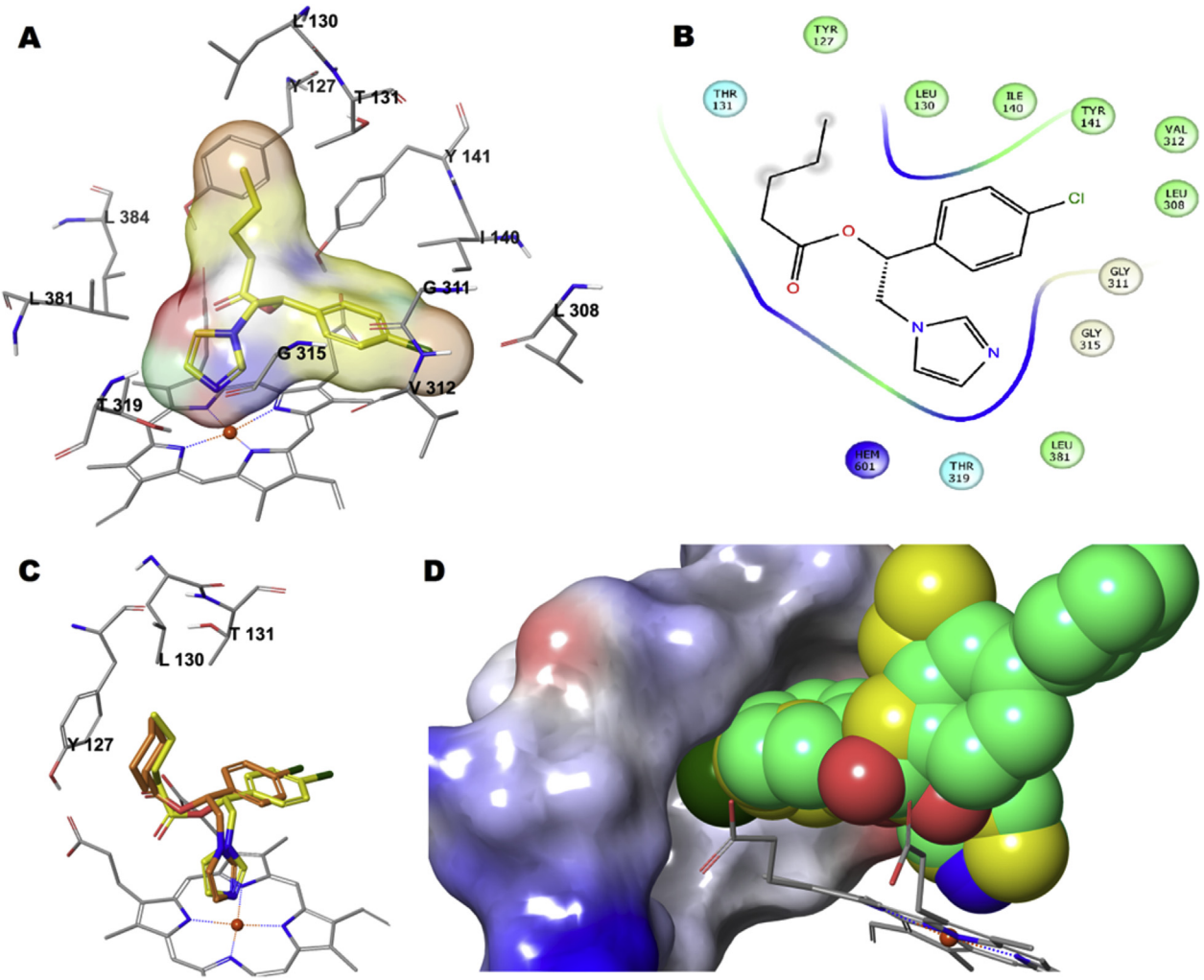

Fig. 6. (double column). Binding interactions of **19** (yellow sticks, surface is rendered) with the active site residues (grey sticks, Fe^{+2} as CPK) of CGCYP51 (**A**); 2-D interaction diagram of **A** (**B**); superposition of **19** (yellow) and **28** (orange) in CACYP51 active site (grey sticks, Fe^{+2} as CPK) (**C**); superposition of **19** and **28** (as CPK) in CACYP51 active site (surface of the residues around pharmacophore C is rendered). (For interpretation of the references to colour in this figure legend, the reader is referred to the web version of this article.)

atom and **19**'s C21 atom (d1), as well as the distance between T131's side chain CG2 and C19 of **19** (d2) (Fig. 8). As d1 was around 4.5 Å in the initial conformer it kept quite stable throughout the simulation. However, d2 was far at the beginning, ca. 7 Å and showed a reducing trend as the tail took a flip and ended up around 4.5 Å. This shows that while the tail of **19** kept close to L130 side chain its distance to T131 side chain got closer, maintaining hydrophobic interactions for a while. The conformational flexibility of the aliphatic and alicyclic groups of **19** and **28** in comparison with the rigid planar aromatic groups of other ligands supposedly allowed these compounds to freely interact with the above mentioned residues via their tail. Since there is no mutagenesis data available on key residues of this receptor, we can only theoretically suggest that L130 and T131 could be important residues for CGCYP51 inhibition. The counterparts of these residues in CACYP51 (L121 and Y122) were not in close contact with the docked ligands, nor these residues have been biologically proven to be important for ligand binding so far.

3. Conclusions

In this study we report synthesis and antimicrobial activities of thirty 1-phenyl/1-(4-chlorophenyl)-2-(1*H*-imidazol-1-yl)ethanol ester derivatives, three of which were reported previously in the literature [17,23,24]. The molecular design of the compounds was based on the modification of general structure of (arylalkyl)azole antifungals.

Most of the compounds showed good antifungal activity higher than or comparable to fluconazole against standard fungal strains. Generally, the presence of 4-Cl substituent on the phenyl ring (pharmacophore A) had a positive effect on the activity. In the case of the tail group (pharmacophore C and D), those with aliphatic and aromatic groups were almost equally effective and the presence of additional aromatic group (pharmacophore D) was not crucial for antifungal activity. Structural variations in the alkyl chain of the derivatives with aliphatic tail group did not appear to change the activity. Clinically resistant *C. glabrata* is known to be less susceptible to common antifungal drugs like fluconazole and itraconazole, however some of our compounds proved potent against this

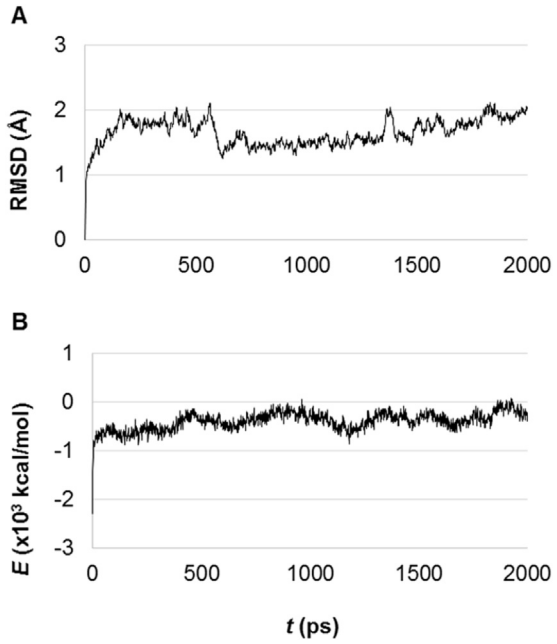

Fig. 7. (single column). Plots of **19**-bound CGCYP51's Cα RMSD values (**A**) and protein total energy (**B**) over time.

species. Surprisingly, those with aliphatic tail were more effective than those with aromatic tail. The efficacy of our compounds was confirmed by biofilm inhibition against biofilm positive *C. albicans* and their safety for human monocytes by cell viability assay. In addition, these compounds, although ester derivatives, are probably not prodrugs. Further studies on chiral separation of the most active compounds, determination of antifungal activities of the pure enantiomers against both *C. albicans* and *C. glabrata*, and prediction of the absolute configuration via molecular modeling are underway.

Using molecular modeling techniques we tried to test some of the suggestions above. For this purpose we built and equilibrated a homology model for CACYP51 and modeled the missing loop of the X-ray structure of CGCYP51. Molecular docking studies on the CACYP51 model revealed key binding interactions for our active compounds in accordance with the available mutagenesis, crystallography, and modeling data. Coordination of with the heme iron via imidazole N and π-π stacking with Y118 and F380 aromatic side chains were observed. The stability of these interactions were confirmed via MD simulations. Molecular docking and MD simulations studies on the CGCYP51 homology model showed the importance of lipophilic interactions with the aliphatic side chain atoms of L130 and T131 for the compounds with aliphatic tail. The interactions of the 4-Cl on the phenyl ring present in **16**–**30** with the active site residues of both models were evident in these studies, as well.

According to these results we suggest that these 1-phenyl/1-(4-chlorophenyl)-2-(1*H*-imidazol-1-yl)ethanol ester derivatives are a worthwhile group to continue to develop new antifungal agents with higher potency and improved safety profile.

4. Experimental section

4.1. Chemistry

4.1.1. Materials and methods

The general synthesis of **1**–**30** is depicted in Scheme 1. All reagents and solvents were obtained from commercial suppliers and used as purchased. All reactions were monitored by analytical thin-

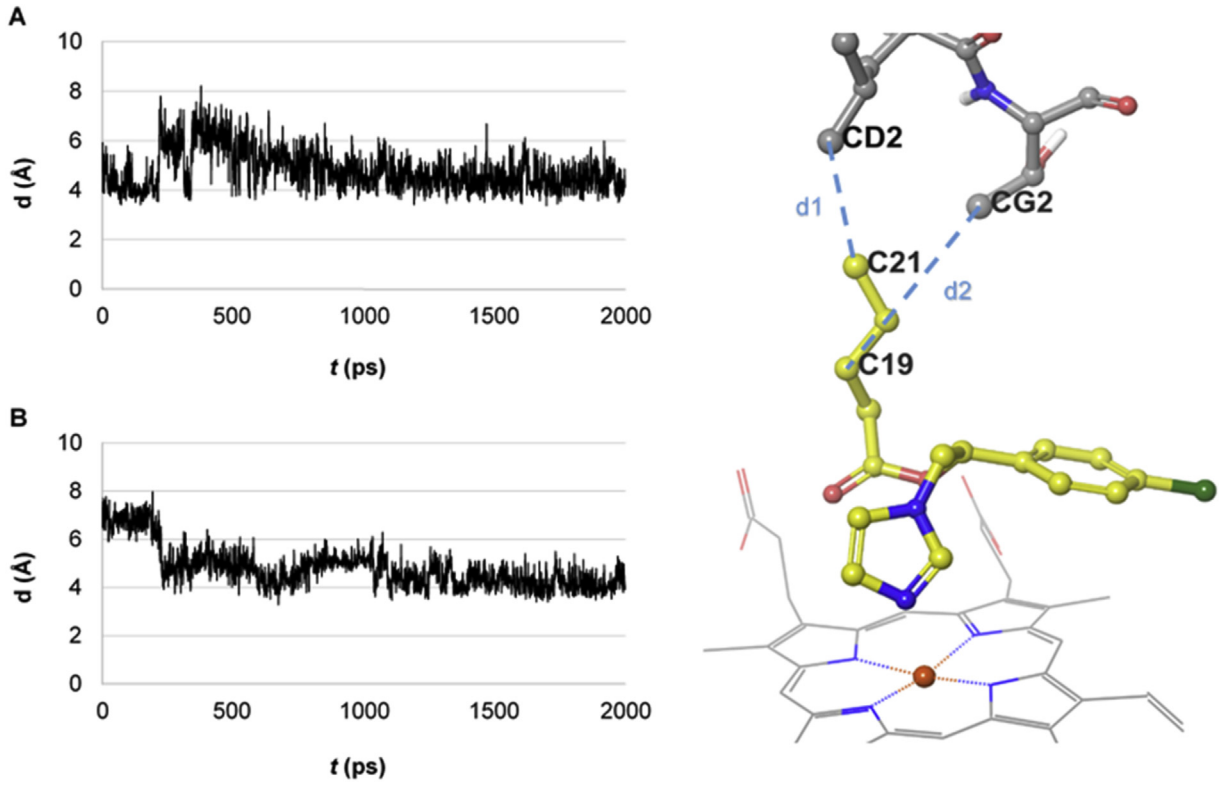

Fig. 8. (1.5 column). Time-dependent change of d1 (CD2-C21) (**A**) and d2 (CG2-c19Cα) (**B**) values of **19**-bound CGCYP51.

layer chromatography using Merck pre-coated silica gel plates with F254 indicator. Column chromatography was performed using Merck silica gel 60 (230–400 mesh ASTM) as stationary phase and chloroform/methanol (90:10) as solvent system. Melting points (mp) were measured on a Thomas Hoover capillary melting point apparatus and uncorrected. ^{1}H and ^{13}C NMR spectra were recorded on a Varian Mercury 400, 400 MHz Digital FT-NMR instrument with tetramethylsilane as an internal standard. Chemical shifts (δ) are reported in parts per million (ppm) and coupling constants (J) in Hertz with multiplicities described as s = singlet, d = doublet, t = triplet, q = quartet, and m = multiplet. IR spectra were recorded on a Perkin Elmer Spectrum BX FT-IR spectrophotometer using attenuated total reflectance (ATR) FT-IR method. Mass spectrometry was conducted using a Micromass ZQ LC-MS spectrometer (ESI + mode) connected with Waters Alliance HPLC. Elemental analyses were performed on a Leco CHNS-932 elemental analyzer. Analyses indicated by the symbols of the elements or functions were within ±0.4% of the theoretical values.

4.1.2. Preparation of compounds

4.1.2.1. 2-Bromo-1-phenyl/1-(4-chlorophenyl)ethanone [40]. To the solution of acetophenone or 4-chloroacetophenone (50 mmol) in acetic acid added dropwise first 3 drops of HBr then 50 mmol Br_2 solution in 2.5 mL acetic acid by vigorously stirring at 0–5 °C. The reaction mixture was warmed to room temperature and allowed to stir for 2 h then poured into ice water. The precipitate was filtered, washed with sodium bicarbonate solution, dried in dark, and crystallized from methanol/water (2-bromo-1-phenylethanone, mp 46 °C; 2-bromo-1-(4-chlorophenyl)ethanone, mp 92 °C).

4.1.2.2. 1-Phenyl/1-(4-chlorophenyl)-2-(1H-imidazol-1-yl)ethanone [41]. To a solution of imidazole (30 mmol) in 2.5 mL DMF was added dropwise 2-bromo-1-phenyl/1-(4-chlorophenyl)ethanone (10 mmol) solution in 2.5 mL DMF by vigorously stirring at 0–5 °C. The reaction mixture was allowed to stir for an additional 2 h at 0–5 °C then at room temperature overnight then poured into ice water. The resulting precipitate was filtered, dried, and purified via crystallization from ethyl acetate/ethanol and ethanol. (1-Phenyl-2-(1*H*-imidazol-1-yl)ethanone, mp 109-10 °C; 1-(4-chlorophenyl)-2-(1*H*-imidazol-1-yl)-ethanone, mp 156-8 °C).

4.1.2.3. Synthesis of 1-phenyl/1-(4-chlorophenyl)-2-(1H-imidazol-1-yl)ethanol [41].

1-Phenyl/1-(4-chlorophenyl)-2-(1*H*-imidazol-1-yl)ethanone (1.8 mmol) solution in methanol was treated with $NaBH_4$ (5.4 mmol) and the reaction mixture was stirred for 1 h at 0–5 °C. Methanol was evaporated, the residue was treated with ice water. The precipitate was filtered and purified via crystallization from ethyl acetate/ethanol and ethanol. (1-Phenyl-2-(1*H*-imidazol-1-yl) ethanol, mp 147 °C; 1-(4-chlorophenyl)-2-(1*H*-imidazol-1-yl) ethanol, mp 181-2 °C).

4.1.2.4. 1-Phenyl/1-(4-chlorophenyl)-2-(1H-imidazol-1-yl)ethanol esters (1-30) [42]. Equimolar amounts (2.5 mmol) of appropriate carboxylic acid and 1-phenyl/1-(4-chlorophenyl)-2-(1*H*-imidazol-1-yl)ethanol were stirred in dry DCM, a solution of DCC (2.5 mmol) and DMAP (0.17 mmol) in dry DCM (5 mL) were added dropwise at 0–5 °C. The reaction mixture was stirred for 0.5 h then warmed to room temperature and stirred for an additional 6 h. The resulting precipitate was filtered off, the filtrate was dried over anhydrous sodium sulphate, and DCM was evaporated to dryness. The residue was purified by column chromatography and converted to its HCl salt by treating with ethereal hydrochloric acid (except **21**).

*4.1.2.4.1. 1-Phenyl-2-(1H-imidazol-1-yl)ethyl acetate hydrochloride **(1)**.* General procedure was followed using 2-(1*H*-imidazol-1-yl)-1-phenylethanol and acetic acid to give the title compound **1** as an off-white solid (yield 11%; mp 175-6 °C). ^{1}H NMR (400 MHz, $CHCl_3$-d) δ 2.11 (s, 3H, -C$\underline{H}_3$), 4.63–4.68 (dd, 1H, J_{AB}: 14.4 Hz, J_{AX}: 7.6 Hz, -C$\underline{H}_2$-N H_A), 4.79–4.84 (dd, 1H, J_{AB}: 14.4 Hz, J_{BX}: 3.6 Hz, -C$\underline{H}_2$-N H_B), 6.18–6.20 (dd, 1H, J_{AX}: 7.2 Hz, J_{BX}: 4 Hz, -C$\underline{H}$-O H_X), 7.07 (s, 1H, imidazole H_4), 7.28 (s, 1H, imidazole H_5), 7.35 (s, 5H, phenyl protons), 9.53 (s, 1H, imidazole H_2). IR (KBr, ν/cm^{-1}): 1729 (C=O, ester). MS (ESI$^+$) *m/z*: 254 (M + Na + H), 253 (M + Na, base peak, 100%), 231, 171, 163. Elemental analysis calculated (%) for $C_{13}H_{14}N_2O_2$. HCl. 0.2 H_2O: C 57.76, H 5.74, N 10.36. Found: C 58.10, H 5.95, N 10.46.

*4.1.2.4.2. 1-Phenyl-2-(1H-imidazol-1-yl)ethyl propionate hydrochloride **(2)**.* General procedure was followed using 2-(1*H*-imidazol-1-yl)-1-phenylethanol and propionic acid to give the title compound **2** as an off-white solid (yield 25%; mp 121-2 °C). ^{1}H NMR (400 MHz, $CHCl_3$-d) δ 1.11 (t, 3H, J_{ab}: 7.2 Hz, -C$\underline{H}_3$ H_a), 2.37–2.43 (q, 2H, J_{ab}: 7.2 Hz, -C$\underline{H}_2$-CH_3 H_b), 4.64–4.68 (dd, 1H, J_{AB}: 13.6 Hz, J_{AX}: 6.8 Hz, CH_2-N H_A), 4.77–4.80 (d, 1H, J_{AB}: 13.6 Hz, C$\underline{H}_2$-N H_B), 6.18 (t, 1H, J_{AX}: 6.8 Hz, -C$\underline{H}$-O H_X), 7.03 (s, 1H, imidazole H_4), 7.27 (s, 1H, imidazole H_5), 7.31–7.36 (m, 5H, phenyl protons), 9.45 (s, 1H, imidazole H_2). ^{13}C NMR (400 MHz, $CHCl_3$-d) δ 9.12 (C$\underline{H}_3$), 27.74 (C$\underline{H}_2$-CH_3), 53.92 (CH_2-N), 73.40 (CH-O), 119.59 (imidazole C-5), 121.45 (imidazole C-4), 126.16 (phenyl C-2, C-4, C-6), 129.12 (phenyl C-3), 129.24 (phenyl C-5), 135.32 (imidazole C-2), 136.19 (phenyl C-1), 172.78 (ester C=O). IR (KBr, ν/cm^{-1}): 1735 (C=O, ester). MS (ESI$^+$) *m/z*: 245 (M + H, base peak, 100%), 205, 189, 177, 150, 142. Elemental analysis calculated (%) for $C_{14}H_{16}N_2O_2$. HCl. 0.17 H_2O: C 59.26, H 6.16, N 9.87. Found: C 59.12, H 5.81, N 10.26.

*4.1.2.4.3. 1-Phenyl-2-(1H-imidazol-1-yl)ethyl butyrate hydrochloride **(3)**.* General procedure was followed using 2-(1*H*-imidazol-1-yl)-1-phenylethanol and butyric acid to give the title compound **3** as an off-white solid (yield 36%; mp 141-3 °C). ^{1}H NMR (400 MHz, $CHCl_3$-d) δ 0.88 (t, 3H, J_{ab}: 7.2 Hz, -C$\underline{H}_3$ H_a), 1.57–1.63 (m, 2H, -C$\underline{H}_2$-CH_3), 2.35 (t, 2H, J_{ab}: 7.2 Hz, C$\underline{H}_2$-C=O H_b), 4.62–4.67 (dd, 1H, J_{AB}: 14.4 Hz, J_{AX}: 7.6 Hz, -C$\underline{H}_2$-N H_A), 4.76–4.80 (dd, 1H, J_{AB}: 14.4 Hz, J_{BX}: 4 Hz, -C$\underline{H}_2$-N H_B), 6.17–6.20 (dd, 1H, J_{AX}: 7.6 Hz, J_{BX}: 4 Hz, -C$\underline{H}$-O H_X), 7.10 (s, 1H, imidazole H_4), 7.28 (s, 1H, imidazole H_5), 7.34 (s, 5H, phenyl protons), 9.40 (s, 1H, imidazole H_2). IR (KBr, ν/cm^{-1}): 1743 (C=O, ester). MS (ESI$^+$) *m/z*: 282 (M + Na + H), 281 (M + Na, base peak, 100%), 259, 171. Elemental analysis calculated (%) for $C_{15}H_{18}N_2O_2$. HCl. 0.8 H_2O: C 58.27, H 6.72, N 9.06. Found: C 58.05, H 6.72, N 9.12.

*4.1.2.4.4. 1-Phenyl-2-(1H-imidazol-1-yl)ethyl pentanoate hydrochloride **(4)**.* General procedure was followed using 2-(1*H*-imidazol-1-yl)-1-phenylethanol and valeric acid to give the title compound **4** as an off-white solid (yield 15%; mp 105-6 °C). ^{1}H NMR (400 MHz, DMSO-d_6) δ 0.79 (t, 3H, J_{ab}: 7.2 Hz, -C$\underline{H}_3$ H_a), 1.07–1.17 (m, 2H, -C$\underline{H}_2$-CH_3), 1.36–1.44 (m, 2H, -C$\underline{H}_2$-CH_2-C$\underline{H}_3$), 2.32 (t, 2H, J_{bc}: 7.6 Hz, -C$\underline{H}_2$-C=O H_c), 4.64 (d, 2H, J_{AX}: 5.2 Hz, -C$\underline{H}_2$-N H_A), 6.14 (t, 1H, J_{AX}: 5.2 Hz, -C$\underline{H}$-O H_X), 7.34–7.40 (m, 5H, phenyl protons), 7.66 (s, 1H, imidazole H_4), 7.77 (s, 1H, imidazole H_5), 9.19 (s, 1H, imidazole H_2). IR (KBr, ν/cm^{-1}): 1720 (C=O, ester). MS (ESI$^+$) *m/z*: 296 (M + Na + H), 295 (M + Na, base peak, 100%), 273, 205, 171, 151, 84. Elemental analysis calculated (%) for $C_{16}H_{20}N_2O_2$. HCl. 0.2 H_2O: C 61.51, H 6.90, N 8.97. Found: C 61.80, H 6.84, N 9.35.

*4.1.2.4.5. 1-Phenyl-2-(1H-imidazol-1-yl)ethyl 3-methylbutanoate hydrochloride **(5)**.* General procedure was followed using 2-(1*H*-imidazol-1-yl)-1-phenylethanol and isovaleric acid to give the title compound **5** as an off-white solid (yield 20%; mp 99–100 °C). ^{1}H NMR (400 MHz, DMSO-d_6) δ 0.75 (d, 6H, J_{ab}: 3.6 Hz, -($C\underline{H}_3$)$_2$ H_a), 1.85–1.92 (m, 1H, -C$\underline{H}$-(CH_3)$_2$), 2.21 (d, 2H, J_{bc}: 3.6 Hz, -C$\underline{H}_2$-C=O H_c), 4.58–4.68 (m, 2H, -C$\underline{H}_2$-N), 6.11–6.14 (dd, 1H, J_{AX}: 8 Hz, J_{BX}: 4.8 Hz, -C$\underline{H}$-O H_X), 7.35–7.40 (m, 5H, phenyl protons), 7.65 (s, 1H, imidazole H_4), 7.78 (s, 1H, imidazole H_5), 9.16 (s, 1H, imidazole H_2). IR (KBr, ν/cm^{-1}): 1734 (C=O, ester). MS (ESI$^+$) *m/z*: 296 (M + Na + H), 295 (M + Na, base peak, 100%), 273, 247, 205, 171, 84.

Elemental analysis calculated (%) for $C_{16}H_{20}N_2O_2$. HCl: C 62.23, H 6.85, N 9.07. Found: C 62.23, H 6.79, N 9.19.

*4.1.2.4.6. 1-Phenyl-2-(1H-imidazol-1-yl)ethyl 2-propylpentanoate hydrochloride **(6)**.* General procedure was followed using 2-(1*H*-imidazol-1-yl)-1-phenylethanol and valproic acid to give the title compound **6** as an off-white solid (yield 36%; mp 97-9 °C). ^{1}H NMR (400 MHz, DMSO-d_6) δ 0.75 (t, 6H, J_{ab}: 7.2 Hz, -CH_2-C$\underline{H}_3$ H_a), 0.84–1.00 (m, 4H, -CH_2-C$\underline{H}_2$-CH_3), 1.28–1.42 (m, 4H, -C$\underline{H}_2$-CH_2-CH_3), 2.30–2.35 (m, 1H, -C$\underline{H}$-C=O), 4.56–4.61 (dd, 1H, J_{AB}: 14 Hz, J_{AX}: 3.6 Hz, -C$\underline{H}_2$-N H_A), 4.67–4.73 (dd, 1H, J_{AB}: 14.2 Hz, J_{BX}: 10.4 Hz, -C$\underline{H}_2$-N H_B), 6.13–6.16 (dd, 1H, J_{AX}: 3.6 Hz, J_{BX}: 10.2 Hz, -C$\underline{H}$-O H_X), 7.43–7.44 (m, 1H, phenyl protons), 7.72 (t, 1H, imidazole H_4), 7.89 (t, 1H, imidazole H_5), 9.23 (s, 1H, imidazole H_2). IR (KBr, ν/cm^{-1}): 1716 (C=O, ester). MS (ESI$^+$) *m/z*: 338 (M + Na + H), 337 (M + Na, base peak, 100%), 316 (M^++H), 315, 247, 229, 215, 171, 144, 98. Elemental analysis calculated (%) for $C_{19}H_{26}N_2O_2$. HCl. 0.25 H_2O: C 64.21, H 7.80, N 7.88. Found: C 64.48, H 7.84, N 8.00.

*4.1.2.4.7. 1-Phenyl-2-(1H-imidazol-1-yl)ethyl 4-oxopentanoate hydrochloride **(7)**.* General procedure was followed using 2-(1*H*-imidazol-1-yl)-1-phenylethanol and levulinic acid to give the title compound **7** as a light yellow solid (yield 20%; 147-8 °C). ^{1}H NMR (400 MHz, $CHCl_3$-d) δ 2.20 (t, 3H, J_{ab}: 7.2 Hz, -C$\underline{H}_3$ H_a), 2.50–2.55 (dt, 1H, J_{A1B1}: 16.8 Hz, J_{A1A2B2}: 4.4 Hz, -CH_2-C$\underline{H}_2$-CH_3 H_{A1}), 2.64–2.69 (dt, 1H, J_{A1B1}: 16.8 Hz, J_{B1A2B2}: 4.8 Hz, -CH_2-C$\underline{H}_2$-CO-CH_3 H_{B1}), 2.72–2.79 (dt, 1H, J_{A2B2}: 18.8 Hz, J_{A2A1B1}: 4 Hz, -C$\underline{H}_2$-CH_2-CO-CH_3 H_{A2}), 2.89–2.93 (dt, 1H, J_{A2B2}: 18.8 Hz, J_{B2A1B1}: 4.4 Hz, -C$\underline{H}_2$-CH_2-CO-CH_3 H_{B2}), 4.53–4.58 (dd, 1H, J_{AB}: 14.8 Hz, J_{AX}: 5.2 Hz, -C$\underline{H}_2$-N H_A), 4.76–4.80 (dd, 1H, J_{AB}: 14.6 Hz, J_{BX}: 3.2 Hz, -C$\underline{H}_2$-N H_B), 6.20–6.23 (dd, 1H, J_{AX}: 5.4 Hz, J_{BX}: 3.2 Hz, -C$\underline{H}$-O H_X), 7.03 (s, 1H, imidazole H_4), 7.22–7.37 (m, 6H, imidazole H_5 and phenyl protons), 9.06 (s, 1H, imidazole H_2). IR (KBr, ν/cm^{-1}): 1722 (C=O, ester), 1711 (C=O, ketone). MS (ESI$^+$) *m/z*: 310 (M + Na + H), 309 (M + Na, base peak, 100%), 287, 171, 99. Elemental analysis calculated (%) for $C_{16}H_{18}N_2O_3$. HCl: C 59.54, H 5.93, N 8.68. Found: C 59.23, H 5.59, N 8.71.

*4.1.2.4.8. 1-Phenyl-2-(1H-imidazol-1-yl)ethyl hexa-2,4-dienoate hydrochloride **(8)**.* General procedure was followed using 2-(1*H*-imidazol-1-yl)-1-phenylethanol and sorbic acid to give the title compound **8** as a yellow solid (yield 24%; mp 115-6 °C). ^{1}H NMR (400 MHz, DMSO-d_6) δ 1.84 (d, 3H, J_{ab}: 5.2 Hz, -CH=CH-C$\underline{H}_3$ H_a), 4.68 (d, 2H, J_{AX}: 6 Hz, -C$\underline{H}_2$-N H_A), 5.88 (d, 1H, J_{cd}: 12.2 Hz, -CO-C$\underline{H}$=CH- H_d), 6.17 (t, 1H, J_{AX}: 6 Hz, -C$\underline{H}$-O H_X), 6.30–6.32 (m, 1H, -C$\underline{H}$-CH=C$\underline{H}$-CH_3), 7.26–7.32 (m, 1H, -C$\underline{H}$-C$\underline{H}$=CH-CH_3), 7.36–7.42 (m, 6H, -CO-CH=C$\underline{H}$-CH- and phenyl protons), 7.62 (s, 1H, imidazole H_4), 7.73 (s, 1H, imidazole H_5), 9.05 (s, 1H, imidazole H_2). IR (KBr, ν/cm^{-1}): 1719 (C=O, ester). MS (ESI$^+$) *m/z*: 306 (M + Na + H), 305 (M + Na, base peak, 100%), 284 (M^++H), 283, 215, 189, 171, 95. Elemental analysis calculated (%) for $C_{17}H_{18}N_2O_2$. HCl.1/2 H_2O: C 59.01, H 5.97, N 8.10. Found: C 59.41, H 6.06, N 8.27.

*4.1.2.4.9. 1-Phenyl-2-(1H-imidazol-1-yl)ethyl 2-phenylacetate hydrochloride **(9)**.* General procedure was followed using 2-(1*H*-imidazol-1-yl)-1-phenylethanol and phenylacetic acid to give the title compound **9** as an off-white solid (yield 29%; mp 170-1 °C). ^{1}H NMR (400 MHz, DMSO-d_6) δ 3.74 (s, 2H, -C$\underline{H}_2$-C_6H_5), 4.63 (d, 2H, J_{AX}: 6 Hz, -C$\underline{H}_2$-N H_A), 6.14 (t, 1H, J_{AX}: 6 Hz, -C$\underline{H}$-O H_X), 7.17–7.37 (m, 11H, imidazol H_4 and phenyl protons), 7.61 (s, 1H, imidazole H_5), 9.05 (s, 1H, imidazole H_2). IR (KBr, ν/cm^{-1}): 1718 (C=O, ester). MS (ESI$^+$) *m/z*: 330 (M + Na + H), 329 (M + Na, base peak, 100%), 307, 182, 171, 151, 91. Elemental analysis calculated (%) for $C_{19}H_{18}N_2O_2$. HCl: C 66.57, H 5.59, N 8.17. Found: C 66.77, H 5.49, N 8.28.

*4.1.2.4.10. 1-Phenyl-2-(1H-imidazol-1-yl)ethyl 4-phenylbutanoate hydrochloride **(10)**.* General procedure was followed using 2-(1*H*-imidazol-1-yl)-1-phenylethanol and 4-phenylbutanoic acid to give the title compound **10** as an off-white solid (yield 20%; mp 119-20 °C). ^{1}H NMR (400 MHz, DMSO-d_6) δ 1.72–1.79 (m, 2H, -CH_2-C$\underline{H}_2$-CH_2-), 2.36 (t, 2H, J_{AX}: 7.2 Hz, -C$\underline{H}_2$-CH_2-CH_2-C_6H_5 H_A), 2.43–2.50 (m, 2H, -C$\underline{H}_2$-C_6H_5), 4.66 (d, 2H, J_{BX}: 7.2 Hz, -C$\underline{H}_2$-N H_B), 6.15–6.18 (dd, 1H, J_{AX}: 4.8 Hz, J_{BX}: 7.8 Hz, -C$\underline{H}$-O H_X), 7.17–7.44 (m, 10H, phenyl protons), 7.67 (t, 1H, J_{ab}: 1.6 Hz, imidazole H_4 H_a), 7.76 (t, 1H, J_{ab}:1.6 Hz, imidazole H_5 H_b), 9.14 (s, 1H, imidazole H_2). IR (KBr, ν/cm^{-1}): 1719 (C=O, ester). MS (ESI$^+$) *m/z*: 358 (M + Na + H), 357 (M + Na, base peak, 100%), 336 (M^++H), 335, 267, 230, 171, 147, 119, 102. Elemental analysis calculated (%) for $C_{21}H_{22}N_2O_2$. HCl: C 68.01, H 6.25, N 7.55. Found: C 67.89, H 6.16, N 7.70.

*4.1.2.4.11. 1-Phenyl-2-(1H-imidazol-1-yl)ethyl 4-oxo-4-phenylbutanoate hydrochloride **(11)**.* General procedure was followed using 2-(1*H*-imidazol-1-yl)-1-phenylethanol and 3-benzoylpropionic acid to give the title compound **11** as a light yellow solid (yield 41%; mp 155-6 °C). ^{1}H NMR (400 MHz, $CHCl_3$-d) δ 2.69–2.76 (dt, 1H, J_{A1B1}: 17 Hz, J_{A1A2B2}: 1.2 Hz, -C$\underline{H}_2$-CH_2-CO-C_6H_5 H_{A1}), 2.84–2.92 (dt, 1H, J_{A1B1}: 16.8 Hz, J_{B1A2B2}: 5.2 Hz, -C$\underline{H}_2$-CH_2-CO-C_6H_5 H_{B1}), 3.27–3.34 (dt, 1H, J_{A2B2}: 18.6 Hz, J_{A2A1B1}: 1.2 Hz, -CH_2-C$\underline{H}_2$-CO-C_6H_5 H_{A2}), 3.44–3.52 (dt, 1H, J_{A2B2}: 18.6 Hz, J_{B2A1B1}: 4.8 Hz, -CH_2-C$\underline{H}_2$-CO-C_6H_5 H_{B2}), 4.54–4.59 (dd, 1H, J_{AB}: 14.4 Hz, J_{AX}: 5.6 Hz, -C$\underline{H}_2$-N H_A), 4.79–4.84 (dd, 1H, J_{AB}: 14.4 Hz, J_{BX}: 3.2 Hz, -C$\underline{H}_2$-N H_B), 6.25–6.27 (dd, 1H, J_{AX}: 5.4 Hz, J_{BX}: 3.2 Hz, -C$\underline{H}$-O H_X), 7.11 (s, 1H, imidazole H_4), 7.23–7.99 (m, 11H, imidazole H_5 and phenyl protons), 9.10 (s, 1H, imidazole H_2). IR (KBr, ν/cm^{-1}): 1733 (C=O, ester), 1672 (C=O, ketone). MS (ESI$^+$) *m/z*: 372 (M + Na + H), 371 (M + Na, base peak, 100%), 349, 171. Elemental analysis calculated (%) for $C_{21}H_{20}N_2O_3$. HCl: C 65.54, H 5.50, N 7.28. Found: C 65.37, H 5.37, N 7.36.

*4.1.2.4.12. 1-Phenyl-2-(1H-imidazol-1-yl)ethyl cinnamate hydrochloride **(12)**.* General procedure was followed using 2-(1*H*-imidazol-1-yl)-1-phenylethanol and *trans*-cinnamic acid to give the title compound **12** as an off-white solid (yield 32%; mp 128-9 °C). ^{1}H NMR (400 MHz, DMSO-d_6) δ 4.73 (d, 2H, J_{AX}: 6.4 Hz, -C$\underline{H}_2$-N H_A), 6.24 (t, 1H, J_{BX}: 6 Hz, -C$\underline{H}$-O H_X), 6.68 (d, 1H, J_{ab}: 15.4 Hz, -C$\underline{H}$=CH-C_6H_5 H_a), 7.43–7.75 (m, 12 H, imidazole H_4, imidazole H_5 and phenyl protons), 7.79 (d, 1H, J_{ab}: 15.4 Hz, -CH=C$\underline{H}$-C_6H_5 H_b), 9.08 (s, 1H, imidazole H_2). IR (KBr, ν/cm^{-1}): 1717 (C=O, ester). MS (ESI$^+$) *m/z*: 342 (M + Na + H), 341 (M + Na, base peak, 100%), 320 (M^++H), 319, 251, 229, 171, 131, 102. Elemental analysis calculated (%) for $C_{20}H_{18}N_2O_2$. HCl. H_2O: C 64.43, H 5.68, N 7.51. Found: C 64.81, H 5.91, N 7.54.

*4.1.2.4.13. 1-Phenyl-2-(1H-imidazol-1-yl)ethyl cyclohexanecarboxylate hydrochloride **(13)**.* General procedure was followed using 2-(1*H*-imidazol-1-yl)-1-phenylethanol and cyclohexanecarboxylic acid to give the title compound **13** as an off-white solid (yield 41%; mp 120-1 °C). ^{1}H NMR (400 MHz, DMSO-d_6) δ 1.02–1.29 (m, 6H, cyclohexane H_3, H_4, H_5), 1.58–1.73 (m, 4H, cyclohexane H_2, H_6), 2.36–2.37 (m, 1H, cyclohexane H_1), 4.64 (d, 2H, J_{AX}: 7.2 Hz, -C$\underline{H}_2$-N H_A), 6.14 (t, 1H, J_{AX}: 7.2 Hz, -C$\underline{H}$-O H_X), 7.37–7.43 (m, 5H, phenyl protons), 7.68 (t, 1H, J_{ab}: 1.6 Hz, imidazole H_4 H_a), 7.79 (t, 1H, J_{ab}: 1.6 Hz, imidazole H_5 H_b), 9.16 (s, 1H, imidazole H_2). IR (KBr, ν/cm^{-1}): 1719 (C=O, ester). MS (ESI$^+$) *m/z*: 322 (M + Na + H), 321 (M + Na, base peak, 100%), 299, 231, 189, 171, 119, 110. Elemental analysis calculated (%) for $C_{18}H_{22}N_2O_2$. HCl. 0.2 H_2O: C 63.88, H 6.97, N 8.28. Found: C 63.96, H 6.92, N 8.49.

*4.1.2.4.14. 1-Phenyl-2-(1H-imidazol-1-yl)ethyl benzoate hydrochloride **(14)**.* General procedure was followed using 2-(1*H*-imidazol-1-yl)-1-phenylethanol and benzoic acid to give the title compound **14** as a light yellow solid (yield 43%; mp 157-8 °C). ^{1}H NMR (400 MHz, DMSO-d_6) δ 4.62–4.70 (dd, 1H, J_{AB}: 14.2 Hz, J_{AX}: 3.6 Hz, -C$\underline{H}_2$-N H_A), 4.74–4.80 (dd, 1H, J_{AB}: 14.4 Hz, J_{BX}: 8.4 Hz, -C$\underline{H}_2$-N H_B), 6.31–6.34 (dd, 1H, J_{AX}: 3.6 Hz, J_{BX}: 8.8 Hz, -C$\underline{H}$-O H_X), 7.35–7.72 (m, 11H, imidazole H_4, imidazole H_5 and phenyl protons), 8.06 (d, 1H, J_{AX}: 5.2 Hz, -CO-$C_6\underline{H}_5$ H_4), 8.69 (s, 1H, imidazole H_2). IR (KBr, ν/cm^{-1}): 1704 (C=O, ester). MS (ESI$^+$) *m/z*: 316 (M + Na + H),

315 (M + Na, base peak, 100%), 309, 293, 225. Elemental analysis calculated (%) for $C_{18}H_{16}N_2O_2$.1/2 HCl.1/2 H_2O: C 67.65, H 5.52, N 8.77. Found: C 67.57, H 5.46, N 8.84.

*4.1.2.4.15. 1-Phenyl-2-(1H-imidazol-1-yl)ethyl 4-biphenylcarboxylate hydrochloride **(15)**.* General procedure was followed using 2-(1*H*-imidazol-1-yl)-1-phenylethanol and 4-biphenylcarboxylic acid to give the title compound **15** as an off-white solid (yield 44%; mp 181-2 °C). ^{1}H NMR (400 MHz, DMSO-d_6) δ 4.74–4.79 (dd, 1H, J_{AB}: 14.6 Hz, J_{AX}: 3.6 Hz, -C$\underline{H}_2$-N H_A), 4.83–4.89 (dd, 1H, J_{AB}: 14.4 Hz, J_{BX}: 8.8 Hz, -C$\underline{H}_2$-N H_B), 6.37–6.40 (dd, 1H, J_{AX}: 3.6 Hz, J_{BX}: 9 Hz, -C$\underline{H}$-O H_X), 7.40–8.14 (m, 16H, imidazole H_4, imidazole H_5 and phenyl protons), 9.12 (s, 1H, imidazole H_2). IR (KBr, ν/cm^{-1}): 1700 (C=O, ester). MS (ESI$^+$) *m/z*: 392 (M + Na + H), 391 (M + Na, base peak, 100%), 370 (M^++H), 369, 301, 247, 181, 171, 151. Elemental analysis calculated (%) for $C_{24}H_{20}N_2O_2\cdot$HCl. 0.67 H_2O: C 69.14, H 5.40, N 6.72. Found: C 69.03, H 5.52, N 6.66.

*4.1.2.4.16. 1-(4-Chlorophenyl)-2-(1H-imidazol-1-yl)ethyl acetate hydrochloride **(16)**.* General procedure was followed using 2-(1*H*-imidazol-1-yl)-1-(4-chlorophenyl)ethanol and acetic acid to give the title compound **16** as an off-white solid (yield 10%; mp 198-9 °C). ^{1}H NMR (400 MHz, $CHCl_3$-d) δ 2.11 (s, 3H, -C$\underline{H}_3$), 4.60–4.66 (dd, 1H, J_{AB}: 14.6 Hz, J_{AX}: 7.6 Hz, -C$\underline{H}_2$-N H_A), 4.80–4.84 (dd, 1H, J_{AB}: 14.4 Hz, J_{BX}: 4 Hz, -C$\underline{H}_2$-N H_B), 6.15–6.18 (dd, 1H, J_{AX}: 7.8 Hz, J_{BX}: 3.6 Hz, -C$\underline{H}$-O H_X), 7.05 (s, 1H, imidazole H_4), 7.26 (s, 1H, imidazole H_5), 7.34 (d, 4H, J_{AB}: 8.4 Hz, phenyl protons H_A), 9.67 (s, 1H, imidazole H_2). IR (KBr, ν/cm^{-1}): 1733 (C=O, ester). MS (ESI$^+$) *m/z*: 289 (M + Na+2), 287 (M + Na, base peak, 100%), 265, 253, 206, 196, 151. Elemental analysis calculated (%) for $C_{13}H_{13}ClN_2O_2\cdot$HCl: C 51.84, H 4.69, N 9.30. Found: C 52.16, H 4.85, N 9.39.

*4.1.2.4.17. 1-(4-Chlorophenyl)-2-(1H-imidazol-1-yl)ethyl propionate hydrochloride **(17)**.* General procedure was followed using 2-(1*H*-imidazol-1-yl)-1-(4-chlorophenyl)ethanol and propionic acid to give the title compound **17** as an off-white (yield 31%; mp 161-3 °C). ^{1}H NMR (400 MHz, $CHCl_3$-d) δ 1.09 (t, 3H, J_{ab}: 7.2 Hz, -C$\underline{H}_3$ H_a), 2.35–2.41 (q, 2H, J_{ab}: 7.2 Hz, -C$\underline{H}_2$-CH_3 H_b), 4.63–4.69 (dd, 1H, J_{AB}: 14.4 Hz, J_{AX}: 8.4 Hz, -C$\underline{H}_2$-N H_A), 4.83–4.88 (dd, 1H, J_{AB}: 14.4 Hz, J_{BX}: 3.6 Hz, -C$\underline{H}_2$-N H_B), 6.18–6.21 (dd, 1H, J_{AX}: 7.8 Hz, J_{BX}: 3.6 Hz, -C$\underline{H}$-O H_X), 7.12 (s, 1H, imidazole H_4), 7.27 (s, 1H, imidazole H_5), 7.32–7.38 (m, 4H, phenyl protons), 9.76 (s, 1H, imidazole H_2). IR (KBr, ν/cm^{-1}): 1741 (C=O, ester). MS (ESI$^+$) *m/z*: 303 (M + Na+2), 301 (M + Na, base peak, 100%), 279, 267, 211, 204, 151. Elemental analysis calculated (%) for $C_{14}H_{15}ClN_2O_2\cdot$HCl: C 53.35, H 5.12, N 8.89. Found: C 53.27, H 5.34, N 8.92.

*4.1.2.4.18. 1-(4-Chlorophenyl)-2-(1H-imidazol-1-yl)ethyl butyrate hydrochloride **(18)**.* General procedure was followed using 2-(1*H*-imidazol-1-yl)-1-(4-chlorophenyl)ethanol and butyric acid to give the title compound **18** as an off-white solid (yield 21%; mp 98-9 °C). ^{1}H NMR (400 MHz, $CHCl_3$-d) δ 0.88 (t, 3H, J_{ab}: 7.2 Hz, -C$\underline{H}_3$ H_a), 1.57–1.63 (m, 2H, -C$\underline{H}_2$-CH_3), 2.34 (t, 2H, J_{ab}: 7.2 Hz, -C$\underline{H}_2$-C=O H_b), 4.61–4.67 (dd, 1H, J_{AB}: 14.4 Hz, J_{AX}: 8 Hz, -C$\underline{H}_2$-N H_A), 4.79–4.83 (dd, 1H, J_{AB}: 14.4 Hz, J_{BX}: 3.2 Hz, -C$\underline{H}_2$-N H_B), 6.16–6.19 (dd, 1H, J_{AX}: 8 Hz, J_{BX}: 3.6 Hz, -C$\underline{H}$-O H_X), 7.08 (s, 1H, imidazole H_4), 7.26 (s, 1H, imidazole H_5), 7.35 (d, 4H, J_{AB}: 6 Hz, phenyl protons H_A), 9.64 (s, 1H, imidazole H_2). IR (KBr, ν/cm^{-1}): 1746 (C=O, ester). MS (ESI$^+$) *m/z*: 317 (M + Na+2), 315 (M + Na, base peak, 100%), 293, 281, 225, 205. Elemental analysis calculated (%) for $C_{15}H_{17}ClN_2O_2\cdot$HCl·$H_2O$: C 51.88, H 5.81, N 8.07. Found: C 51.69, H 5.70, N 8.20.

*4.1.2.4.19. 1-(4-Chlorophenyl)-2-(1H-imidazol-1-yl)ethyl pentanoate hydrochloride **(19)**.* General procedure was followed using 2-(1*H*-imidazol-1-yl)-1-(4-chlorophenyl)ethanol and valeric acid to give the title compound **19** as an off-white solid (yield 24%; mp 109-10 °C). ^{1}H NMR (400 MHz, $CHCl_3$-d) δ 0.88 (t, 3H, J_{ab}: 7.2 Hz, -C$\underline{H}_3$ H_a), 1.24–1.29 (m, 2H, -C$\underline{H}_2$-CH_3), 1.50–1.56 (m, 2H, -C$\underline{H}_2$-CH_2-CH_3), 2.35 (t, 2H, J_{ab}: 7.2 Hz, -C$\underline{H}_2$-C=O H_b), 4.62–4.68 (dd, 1H, J_{AB}: 14.2 Hz, J_{AX}: 8.4 Hz, -C$\underline{H}_2$-N H_A), 4.82–4.86 (dd, 1H, J_{AB}: 14.6 Hz, J_{BX}: 3.6 Hz, -C$\underline{H}_2$-N H_B), 6.17–6.20 (dd, 1H, J_{AX}: 8.2 Hz, J_{BX}: 3.6 Hz, -C$\underline{H}$-O H_X), 7.12 (s, 1H, imidazole H_4), 7.27 (s, 1H, imidazole H_5), 7.34 (d, 4H, phenyl protons), 9.72 (s, 1H, imidazole H_2). IR (KBr, ν/cm^{-1}): 1741 (C=O, ester). MS (ESI$^+$) *m/z*: 331 (M + Na+2), 329 (M + Na, base peak, 100%), 307, 295, 205, 84. Elemental analysis calculated (%) for $C_{16}H_{19}ClN_2O_2\cdot$HCl: C 55.99, H 5.87, N 8.16. Found: C 55.92, H 5.77, N 8.28.

*4.1.2.4.20. 1-(4-Chlorophenyl)-2-(1H-imidazol-1-yl)ethyl 3-methylbutanoate hydrochloride **(20)**.* General procedure was followed using 2-(1*H*-imidazol-1-yl)-1-(4-chlorophenyl)ethanol and isovaleric acid to give the title compound **20** as an off-white solid (yield 31%; mp 148-9 °C). ^{1}H NMR (400 MHz, $CHCl_3$-d) δ 0.87 (d, 6H, J_{ab}: 3.6 Hz, -($C\underline{H}_3$)$_2$ H_a), 2.01–2.05 (m, 1H, -C$\underline{H}$-(CH_3)$_2$), 2.22 (d, 2H, J_{bc}: 7.6 Hz, -C$\underline{H}_2$-C=O H_c), 4.63–4.68 (dd, 1H, J_{AB}: 14.4 Hz, J_{AX}: 8.4 Hz, -C$\underline{H}_2$-N H_A), 4.79–4.83 (dd, 1H, J_{AB}: 14.6 Hz, J_{BX}: 4 Hz, -C$\underline{H}_2$-N H_B), 6.16–6.19 (dd, 1H, J_{AX}: 8.2 Hz, J_{BX}: 4 Hz, -C$\underline{H}$-O H_X), 7.09 (s, 1H, imidazole H_4), 7.26 (s, 1H, imidazole H_5), 7.35 (d, 4H, J: 8.4 Hz, phenyl protons), 9.68 (s, 1H, imidazole H_2). IR (KBr, ν/cm^{-1}): 1733 (C=O, ester). MS (ESI$^+$) *m/z*: 331 (M + Na+2), 329 (M + Na, base peak, 100%), 309 (M+2), 307, 295, 273, 239, 205, 182, 155, 102, 84. Elemental analysis calculated (%) for $C_{16}H_{19}ClN_2O_2\cdot$HCl: C 55.99, H 5.87, N 8.16. Found: C 55.83, H 5.66, N 8.27.

*4.1.2.4.21. 1-(4-Chlorophenyl)-2-(1H-imidazol-1-yl)ethyl 2-propylpentanoate **(21)**.* General procedure was followed using 2-(1*H*-imidazol-1-yl)-1-(4-chlorophenyl)ethanol and valproic acid to give the title compound **21** as an off-white solid (yield 25%; mp 99–100 °C). ^{1}H NMR (400 MHz, DMSO-d_6) δ 0.75 (t, 6H, J_{ab}: 6.8 Hz, -CH_2-C$\underline{H}_3$ H_a), 0.96–1.17 (m, 4H, -CH_2-C$\underline{H}_2$-CH_3), 1.23–1.64 (m, 4H, -C$\underline{H}_2$-CH_2-CH_3), 1.82–2.50 (m, 1H, -C$\underline{H}$-C=O), 4.60–4.63 (m, 2H, -C$\underline{H}_2$-N), 6.13–6.17 (dd, 1H, J_{AX}: 9.6 Hz, J_{BX}: 3.2 Hz, -C$\underline{H}$-O H_X), 6.88–7.54 (m, 4H, phenyl protons), 7.74 (t, 1H, J_{ab}: 1.2 Hz, imidazole H_4 H_a), 7.89 (t, 1H, J_{ab}: 1.6 Hz, imidazole H_5 H_b), 9.27 (s, 1H, imidazole H_2). IR (KBr): 1716 (C=O, ester). MS (ESI$^+$) *m/z*: 372 (M + Na+2), 371 (M + Na), 349, 315, 279, 263, 247 (base peak, 100%), 205, 177, 121, 102. Elemental analysis calculated (%) for $C_{19}H_{25}ClN_2O_2$: C 65.41, H 7.22, N 8.03. Found: C 65.13, H 7.62, N 8.29.

*4.1.2.4.22. 1-(4-Chlorophenyl)-2-(1H-imidazol-1-yl)ethyl 4-oxopentanoate hydrochloride **(22)**.* General procedure was followed using 2-(1*H*-imidazol-1-yl)-1-(4-chlorophenyl)ethanol and levulinic acid to give the title compound **22** as a light yellow solid (yield 26%; mp 143-4 °C). ^{1}H NMR (400 MHz, $CHCl_3$-d) δ 2.18 (s, 3H, -C$\underline{H}_3$), 2.49–2.56 (dt, 1H, J_{A1B1}: 16.8 Hz, J_{A1A2B2}: 5.4 Hz, -CH_2-C$\underline{H}_2$-CO-CH_3 H_{A1}), 2.61–2.68 (dt, 1H, J_{A1B1}: 16.8 Hz, J_{B1A2B2}: 4.4 Hz, -CH_2-C$\underline{H}_2$-CO-CH_3 H_{B1}), 2.70–2.77 (dt, 1H, J_{A2B2}: 18.8 Hz, J_{A2A1B1}: 5.4 Hz, -C$\underline{H}_2$-CH_2-CO-CH_3 H_{A2}), 2.83–2.90 (dt, 1H, J_{A2B2}: 18.8 Hz, J_{B2A1B1}: 4.4 Hz, -C$\underline{H}_2$-CH_2-CO-CH_3 H_{B2}), 4.61–4.67 (dd, 1H, J_{AB}: 14.6 Hz, J_{AX}: 6.4 Hz, -C$\underline{H}_2$-N H_A), 4.82–4.86 (dd, 1H, J_{AB}: 14.8 Hz, J_{BX}: 3.2 Hz, -C$\underline{H}_2$-N H_B), 6.19–6.21 (t, 1H, J_{AX}: 6.6 Hz, J_{BX}: 3.2 Hz, -C$\underline{H}$-O H_X), 7.16 (s, 1H, imidazole H_4), 7.27 (s, 1H, imidazole H_5), 7.29–7.36 (m, 4H, phenyl protons), 9.52 (s, 1H, imidazole H_2). IR (KBr, ν/cm^{-1}): 1725 (C=O, ester). MS (ESI$^+$) *m/z*: 345 (M + Na+2), 343 (M + Na base peak, 100%), 321, 309, 205, 151. Elemental analysis calculated (%) for $C_{16}H_{17}ClN_2O_3\cdot$HCl·1/3$H_2O$: C 52.91, H 5.18, N 7.71. Found: C 53.26, H 5.08, N 7.83.

*4.1.2.4.23. 1-(4-Chlorophenyl)-2-(1H-imidazol-1-yl)ethyl hexa-2,4-dienoate hydrochloride **(23)**.* General procedure was followed using 2-(1*H*-imidazol-1-yl)-1-(4-chlorophenyl)ethanol and sorbic acid to give the title compound **23** as a yellow solid (yield 21%; mp 140-1 °C). ^{1}H NMR (400 MHz, DMSO-d_6) δ 1.83 (d, 3H, J_{ab}: 4.8 Hz, -CH=CH-C$\underline{H}_3$ H_a), 4.70 (d, 2H, J_{AX}: 6.4 Hz, -C$\underline{H}_2$-N H_A), 5.88 (1H, d, J_{cd}: 14.2 Hz, -CO-C$\underline{H}$=CH- H_d), 6.19 (t, 1H, J_{AX}: 6 Hz, -C$\underline{H}$-O H_X), 6.30–6.33 (m, 1H, -CH-CH=C$\underline{H}$-CH_3), 7.27–7.34 (m, 1H, -CH-C$\underline{H}$=CH-CH_3), 7.41–7.51 (m, 5H, -CO-CH=C$\underline{H}$-CH- and phenyl protons), 7.65 (s, 1H, imidazole H_4), 7.75 (s, 1H, imidazole H_5), 9.16 (s,

1H, imidazole H_2). IR (KBr, ν/cm^{-1}): 1720 (C=O, ester). MS (ESI$^+$) *m/z*: 341 (M + Na+2), 339 (M + Na base peak, 100%), 318 (M$^+$+H), 317, 263, 249, 205, 185, 95. Elemental analysis calculated (%) for $C_{17}H_{17}ClN_2O_2 \cdot HCl \cdot 1/2H_2O$: C 56.36, H 5.29, N 7.73. Found: C 56.22, H 5.03, N 7.76.

4.1.2.4.24. 1-(4-Chlorophenyl)-2-(1H-imidazol-1-yl)ethyl 2-phenylacetate hydrochloride ***(24)***. General procedure was followed using 2-(1*H*-imidazol-1-yl)-1-(4-chlorophenyl)ethanol and phenylacetic acid to give the title compound **24** as a yellow solid (yield 26%; mp 104-5 °C). ^{1}H NMR (400 MHz, DMSO-d_6) δ 3.75 (s, 2H, -C$\underline{H}_2$-C_6H_5), 4.65 (d, 2H, J_{AX}: 6 Hz, -C$\underline{H}_2$-N H_A), 6.16 (t, 1H, J_{BX}: 5.6 Hz, -C$\underline{H}$-O H_X), 7.19–7.61 (m, 11H, imidazole H_4, imidazole H_5 and phenyl protons), 9.05 (s, 1H, imidazole H_2). IR (KBr, ν/cm^{-1}): 1717 (C=O, ester). MS (ESI$^+$) *m/z*: 365 (M + Na+2), 363 (M + Na base peak, 100%), 343 (M+2), 341, 307, 273, 229, 205, 118, 102. Elemental analysis calculated (%) for $C_{19}H_{17}ClN_2O_2 \cdot HCl$: C 60.49, H 4.81, N 7.43. Found: C 60.70, H 4.75, N 7.55.

4.1.2.4.25. 1-(4-Chlorophenyl)-2-(1H-imidazol-1-yl)ethyl 4-phenylbutanoate hydrochloride ***(25)***. General procedure was followed using 2-(1*H*-imidazol-1-yl)-1-(4-chlorophenyl)ethanol and 4-phenylbutanoic acid to give the title compound **25** as an off-white solid (yield 25%; mp 141-2 °C). ^{1}H NMR (400 MHz, DMSO-d_6) δ 1.72–1.80 (m, 2H, CH_2-C$\underline{H}_2$-CH_2), 2.37 (t, 2H, J_{AX}: 7.2 Hz, -C$\underline{H}_2$-CH_2-CH_2-C_6H_5 H_A), 2.44–2.53 (m, 2H, -C$\underline{H}_2$-C_6H_5), 4.67 (t, 2H, J_{AX}: 4.4 Hz, -C$\underline{H}_2$-N H_A), 6.16–6.19 (dd, 1H, J_{AX}: 4.4 Hz, J_{BX}: 7 Hz, -CH-O H_X), 7.12–7.51 (m, 9H, phenyl protons), 7.67 (s, 1H, imidazole H_4), 7.75 (s, 1H, imidazole H_5), 9.17 (s, 1H, imidazole H_2). IR (KBr, ν/cm^{-1}): 1719 (C=O, ester). MS (ESI$^+$) *m/z*: 393 (M + Na+2), 391 (M + Na base peak, 100%), 371 (M+2), 369, 335, 301, 287, 245, 229, 205, 147, 120, 102. Elemental analysis calculated (%) for $C_{21}H_{21}ClN_2O_2 \cdot HCl$: C 62.23, H 5.47, N 6.91. Found: C 62.15, H 5.25, N 7.01.

4.1.2.4.26. 1-(4-Chlorophenyl)-2-(1H-imidazol-1-yl)ethyl 4-oxo-4-phenylbutanoate ***(26)***. General procedure was followed using 2-(1*H*-imidazol-1-yl)-1-(4-chlorophenyl)ethanol and 3-benzoylpropionic acid to give the title compound **26** as a light yellow solid base (yield 14%; mp 88-9 °C). ^{1}H NMR (400 MHz, $CHCl_3$-d) δ 2.69–2.76 (dt, 1H, J_{A1B1}: 16.8 Hz, J_{A1A2B2}: 4.8 Hz, -C$\underline{H}_2$-CH_2-CO-C_6H_5 H_{A1}), 2.80–2.88 (dt, 1H, J_{A1B1}: 16.8 Hz, J_{B1A2B2}: 4.4 Hz, -C$\underline{H}_2$-CH_2-CO-C_6H_5 H_{B1}), 3.24–3.31 (dt, 1H, J_{A2B2}: 18.8 Hz, J_{A2A1B1}: 4.8 Hz, -CH_2-C$\underline{H}_2$-CO-C_6H_5 H_{A2}), 3.37–3.45 (dt, 1H, J_{A2B2}: 18.6 Hz, J_{B2A1B1}: 4.8 Hz, -CH_2-C$\underline{H}_2$-CO-C_6H_5 H_{B2}), 4.61–4.66 (dd, 1H, J_{AB}: 14.6 Hz, J_{AX}: 6.4 Hz, -C$\underline{H}_2$-N H_A), 4.83–4.88 (dd, 1H, J_{AB}: 14.4 Hz, J_{BX}: 3.2 Hz, -C$\underline{H}_2$-N H_B), 6.23–6.25 (t, 1H, J_{AX}: 6.6 Hz, J_{BX}: 3.2 Hz, -C$\underline{H}$-O H_X), 7.21 (s, 1H, imidazole H_4), 7.26 (s, 1H, imidazole H_5), 7.29–7.96 (m, 9H, phenyl protons), 9.52 (s, 1H, imidazole H_2). IR (KBr, ν/cm^{-1}): 1732 (C=O, ester), 1676 (C=O, ketone). MS (ESI$^+$) *m/z*: 407 (M + Na+2), 405 (M + Na base peak, 100%), 385 (M+2), 383, 204, 182, 151, 119, 102. Elemental analysis calculated (%) for $C_{21}H_{19}ClN_2O_3$: C 65.88, H 5.00, N 7.32. Found: C 65.61, H 5.16, N 7.32.

4.1.2.4.27. 1-(4-Chlorophenyl)-2-(1H-imidazol-1-yl)ethyl cinnamate hydrochloride ***(27)***. General procedure was followed using 2-(1*H*-imidazol-1-yl)-1-(4-chlorophenyl)ethanol and *trans*-cinnamic acid to give the title compound **27** as an off-white solid (yield 18%; mp 113-4 °C). ^{1}H NMR (400 MHz, DMSO-d_6) δ 4.76 (d, 2H, J_{AX}: 6 Hz, -C$\underline{H}_2$-N H_A), 6.27 (t, 1H, J_{AX}: 6 Hz, -C$\underline{H}$-O H_X), 6.69 (d, 1H, J_{ab}: 16.4 Hz, -C$\underline{H}$=CH-C_6H_5 H_a), 7.45–7.78 (m, 11H, imidazole H_4, imidazole H_5 and phenyl protons), 7.81 (d, 1H, J_{ab}: 16.4 Hz, -CH=C$\underline{H}$-C_6H_5 H_b), 9.24 (s, 1H, imidazole H_2). IR (KBr, ν/cm^{-1}): 1717 (C=O, ester). MS (ESI$^+$) *m/z*: 377 (M + Na+2), 375 (M + Na base peak, 100%), 355 (M+2), 353, 285, 247, 205, 185, 118. Elemental analysis calculated (%) for $C_{20}H_{17}ClN_2O_2 \cdot HCl \cdot H_2O$: C 58.98, H 4.95, N 6.88. Found: C 59.17, H 5.17, N 6.91.

4.1.2.4.28. 1-(4-Chlorophenyl)-2-(1H-imidazol-1-yl)ethyl cyclohexanecarboxylate hydrochloride ***(28)***. General procedure was followed using 2-(1*H*-imidazol-1-yl)-1-(4-chlorophenyl)ethanol and cyclohexanecarboxylic acid to give the title compound **28** as an off-white solid (yield 28%; mp 205-6 °C). ^{1}H NMR (400 MHz, DMSO-d_6) δ 1.12–1.27 (m, 6H, cyclohexane H_3, H_4, H_5), 1.55–1.75 (m, 4H, cyclohexane H_2, H_6), 2.35–2.38 (m, 1H, cyclohexane H_1), 4.65 (d, 2H, J_{AX}: 6 Hz, -C$\underline{H}_2$-N H_A), 6.15 (t, 1H, J_{BX}: 5.6 Hz, -C$\underline{H}$-O H_X), 7.42–7.52 (m, 4H, phenyl protons), 7.69 (t, 1H, J_{ab}: 1.6 Hz, imidazole H_4 H_a), 7.79 (t, 1H, J_{ab}: 1.6 Hz, imidazole H_5 H_b), 9.20 (s, 1H, imidazole H_2). IR (KBr, ν/cm^{-1}): 1719 (C=O, ester). MS (ESI$^+$) *m/z*: 357 (M + Na+2), 355 (M + Na base peak, 100%), 335 (M+2), 333, 299, 265, 205, 178, 151, 88. Elemental analysis calculated (%) for $C_{18}H_{21}ClN_2O_2 \cdot HCl$: C 58.54, H 6.00, N 7.59. Found: C 58.27, H 6.07, N 7.65.

4.1.2.4.29. 1-(4-Chlorophenyl)-2-(1H-imidazol-1-yl)ethyl benzoate hydrochloride ***(29)***. General procedure was followed using 2-(1*H*-imidazol-1-yl)-1-(4-chlorophenyl)ethanol and benzoic acid to give the title compound **29** as a light yellow solid (yield 33%; mp 147-8 °C). ^{1}H NMR (400 MHz, DMSO-d_6) δ 4.76–4.80 (dd, 1H, J_{AB}: 14.4 Hz, J_{AX}: 3.6 Hz, -C$\underline{H}_2$-N H_A), 4.84–4.90 (dd, 1H, J_{AB}: 14 Hz, J_{BX}: 8.8 Hz, -C$\underline{H}_2$-N H_B), 6.37–6.40 (dd, 1H, J_{AX}: 3.6 Hz, J_{BX}: 8.6 Hz, -C$\underline{H}$-O H_X), 7.51–8.06 (m, 11H, imidazole H_4, imidazole H_5 and phenyl protons), 9.25 (s, 1H, imidazole H_2). IR (KBr, ν/cm^{-1}): 1730 (C=O, ester). MS (ESI$^+$) *m/z*: 350 (M + Na+2), 349 (M + Na base peak, 100%), 329 (M+2), 327, 247, 205, 182, 151, 105. Elemental analysis calculated (%) for $C_{18}H_{15}ClN_2O_2 \cdot HCl \cdot H_2O$: C 56.71, H 4.76, N 7.35. Found: C 56.53, H 4.98, N 7.29.

4.1.2.4.30. 1-(4-Chlorophenyl)-2-(1H-imidazol-1-yl)ethyl 4-biphenylcarboxylate hydrochloride ***(30)***. General procedure was followed using 2-(1*H*-imidazol-1-yl)-1-(4-chlorophenyl)ethanol and 4-biphenylcarboxylic acid to give the title compound **30** as an off-white solid (yield 24%; mp 122-4 °C). ^{1}H NMR (400 MHz, DMSO-d_6) δ 4.77–4.81 (dd, 1H, J_{AB}: 14 Hz, J_{AX}: 3.6 Hz, -C$\underline{H}_2$-N H_A), 4.85–4.91 (dd, 1H, J_{AB}: 14 Hz, J_{BX}: 8.4 Hz, -C$\underline{H}_2$-N H_B), 6.40–6.43 (dd, 1H, J_{AX}: 3.6 Hz, J_{BX}: 8.6 Hz, -C$\underline{H}$-O H_X), 7.45–8.14 (m, 15H, imidazole H_4, imidazole H_5 and phenyl protons), 9.24 (s, 1H, imidazole H_2). IR (KBr, ν/cm^{-1}): 1698 (C=O, ester). MS (ESI$^+$) *m/z*: 427 (M + Na+2), 425 (M + Na base peak, 100%), 405 (M+2), 403, 369, 335, 247, 205, 181, 151, 102. Elemental analysis calculated (%) for $C_{24}H_{19}ClN_2O_2 \cdot HCl \cdot H_2O$: C 63.03, H 4.85, N 6.13. Found: C 63.37, H 5.09, N 6.21.

4.2. Biological activity

4.2.1. Antimicrobial activity

Antibacterial and antifungal activities of the compounds have been tested against Gram (+) (*Staphylococcus aureus* ATCC 29213, *Enterecoccus faecalis* ATCC 29212) and Gram (-) bacteria (*Escherichia coli* ATCC 25922 and *Pseudomonas aeruginosa* ATCC 27853) and yeast like fungi (*Candida albicans* ATCC 90028 and non-*albicans Candida* species such as *C. krusei* ATCC 6258 and *C. parapsilosis* ATCC 90018) by broth microdilution method. MIC values were determined according to Clinical and Laboratory Standards Institute (CLSI) reference documents [43,44] using ciprofloxacin and fluconazole as reference compounds for antibacterial and antifungal activity, respectively. Isolates stored at −80 °C in glycerol were thawed and subcultured twice onto Mueller Hinton agar for bacteria and Sabouraud dextrose agar for fungi prior to testing. Broth microdilution was performed using Mueller Hinton broth (MHB, Difco Laboratories, Detroit, MI, USA) and RPMI 1640 broth (ICN-Flow, Aurora, OH, USA, with glutamine, without bicarbonate and with pH indicator) buffered to pH 7.0 with 3-N-morpholinopropanesulfonic acid (MOPS; Sigma) for bacteria and yeast, respectively. The inoculum densities were prepared from 24 h subcultures. The final test concentration of bacteria was approximately 5×10^5 cfu/mL and 0.5 to 2.5×10^3 cfu/mL for fungi.

Ciprofloxacin and fluconazole were dissolved in sterile deionized distilled water and used as reference compounds for antibacterial and antifungal activities, respectively (64–0.0625 μg/mL). Compounds **1**-**30** were dissolved in dimethyl sulfoxide (DMSO; Sigma, USA). Final twofold concentrations of the compounds were prepared in the wells of the microtiter plates, between 1024 and 1 μg/mL. The plates were incubated at 35 °C for 18–24 h for bacteria and 48 h for yeast. MIC values were read as the lowest concentration of antimicrobial agent that completely inhibits visual growth of the organism in the wells. The MICs of fluconazole were determined to be at the dilution causing approximately 80% inhibition of growth according to control wells.

4.2.2. Biofilm susceptibility assay/antibiofilm activity

C. albicans biofilms were grown in the Calgary Biofilm Device (commercially available as the MBEC Assay™ for Physiology & Genetics, P & G, Innovotech Inc., Edmonton, Alberta, Canada) according to the MBEC™ assay protocol, a standart ASTM method, as supplied by the manufacturer [45]. In brief, the assay is based on a 96-well microtiter plate. Biofilms are formed on plastic pegs found on the lid of the MBEC device and MBEC values for different antimicrobial agents are determined with these devices.

Aliquots of 150 μl of the final inoculum suspension (106 cfu/mL) were transferred to each of the test wells and the MBEC assay plate lids with 96 pegs were placed into the microtiter plates. The plates were incubated for 24 h at 37 °C to form mature biofilm. After 24 h, the peg lids of the MBEC assay plates were rinsed three times with 100 μl of 0.9% physiological saline (PS), then transferred to a 'challenge' plate. Finally, 200 μl of serial twofold dilutions of each chemical compounds were subsequently added to each well and the wells were incubated for 24 h at 35 °C. The concentration range of the compounds was arranged as 1024-1 μg/mL in columns 1-11, respectively. Positive growth control and sterility control were included in each assay plate. After treatment of the biofilm for 24 h, the peg lids were rinsed three times in 0.9% PS and transferred to a 'recovery' plate, each well contained RPMI 1640 supplemented with 2% glucose. The plates were sonicated for 5 min to remove the biofilms into recovery media and the peg lids were discarded. The recovery plates were incubated overnight and optical densities of the wells were measured at 550 nm by spectrophotometer. The plates were also visually checked after 24 h for turbidity, clear wells were taken as evidence of biofilm eradication. The MBEC values were determined by identifying the lowest antibiotic concentration that prevents regrowth of *C. albicans* from the treated biofilm. MBIC were also determined by identifying the minimum concentration that prevents the initial formation of biofilm checking turbidity visually in the wells.

4.2.3. In vitro cytotoxicity test

The *in vitro* cytotoxicity of compounds **1**-**30** was evaluated on human monocytic cell line (U937) obtained from Hacettepe University, Basic Oncology Department by using 3-(4,5-dimethylthiazol-2-yl)-2,5-diphenyltetrazolium bromide (MTT) reduction assay [46]. The cells (4×10^3 cells/well) were plated into 96 well plates containing 100 μl of RPMI-1640 supplemented with 10% fetal bovine serum, L-glutamine (2 mM), penicillin (50 U/mL), and streptomycin (50 μg/mL) and incubated at 37 °C in 5% CO_2. The cells were exposed to the compounds **1**-**30** at the final concentrations ranging from 10-100 μg/mL (dissolved in DMSO). Each concentration and control were analyzed in three replicates with five final concentrations. The cells and compounds were incubated at 37 °C in 5% CO_2 for 48 h. Twenty μl of MTT solution (5 mg/mL) was added to each well and plates were then incubated at 37 °C in 5% CO_2 for 4 h. 80 μl of sodium dodecyl sulphate (SDS) in 23% DMF was added to the wells to dissolve formazan crystals, and plates were incubated overnight at 37 °C in 5% CO_2. Optical density was measured spectrophotometrically at 570 nm. The cytotoxicity of the compounds was calculated as percentage reduction in viable cells with respect to the control culture cells.

4.3. Molecular modeling studies

4.3.1. Homology modeling of CACYP51 and the missing loop of CGCYP51

We built the structural model of CACYP51 according to comparative modeling methods using MODELLER. We downloaded the crystal structure of *Saccharomyces cerevisiae* CYP51 (PDB id: 5EQB) and CGCYP51 (PDB id: 5JLC) from Protein Data Bank (www.rcsb.org) [47]. A pairwise sequence alignment of CACYP51 (UniProtKB/Swiss-Prot accession code: P10613.2) and 5EQB was generated and manually optimized. Using this alignment and the template structure we constructed 100 initial itraconazole-bound homology models, the best of which was selected upon comparison of their discrete optimized protein energy (DOPE) scores and restraint violations. The selected model was then analyzed using PROCHECK and submitted to the PPM server to determine their membrane-embedded residues. The same protocol was followed for modeling the missing loop of CGCYP51 (residues 435-443) using its full sequence (UniProtKB/Swiss-Prot accession code: P50859.1) and 5JLC as template. The N-terminal residues missing in 5JLC were not modeled. The loop-optimization protocol of MODELLER was applied for the modeled loop. The best model was selected according to the procedures defined for CACYP51.

4.3.2. Molecular dynamics simulations

On VMD [48] we created the systems of ligand-bound CACYP51 and CGCYP51 solvated in water box using CHARMM36 force-field with CMAP corrections for the protein and solvent, and CHARMM General Force-Field (v3.1) via cgenff.paramchem.org server (v1.0) for the ligands [49–54]. A 5 Å (10 Å for CGCYP51) layer of water was added to each face of the box and particle mesh Ewald (PME) method [55] was used. Harmonic potential constraints were imposed on the backbone atoms of the membrane-embedded residues, Fe^{+2} of heme, and S^{-} of heme-coordinating cysteine. Heme was patched to keep planar. Integration time step was 2 fs, SHAKE algorithm was used for hydrogens, and coordinates were saved every 1 ps. Systems were run on NAMD [56] for 2 ns (itraconazole-bound CACYP51 for 1 ns) at constant temperature (310 K) and pressure (1 atm) (NPT ensemble).

4.3.3. Molecular docking

We prepared the ligands using MacroModel (v11.0, Schrödinger, LLC, NY, 2015) and LigPrep (v3.6, Schrödinger, LLC, NY, 2015) of Maestro (v10.4, Schrödinger, LLC, NY, 2015), minimized them using OPLS 2005 force field and conjugate gradients algorithm [57]. For CACYP51, the last frame from itraconazole-bound system's simulation was extracted. We prepared the protein structures for docking using Protein Preparation Wizard of Maestro [58]. In this process explicit water molecules were removed, hydrogens were added, ionization and tautomeric states were generated using Epik (v3.4, Schrödinger, LLC, NY, 2015) [59,60]. We generated grid maps by AutoGrid taking the centroid of the co-crystallized ligands as the center of search space. Ligands were docked using Lamarckian genetic algorithm on AutoDock [61], 50 conformers per each ligand were produced and visually inspected. We used AutoDockTools as graphical user interface for all AutoDock operations and Maestro for inspecting docking poses.

Acknowledgments

This research was financially supported by Hacettepe University Scientific Research Fund (Project no: 010D06301004).

Appendix A. Supplementary data

Supplementary data associated with this article can be found in the online version, at http://dx.doi.org/10.1016/j.ejmech.2017.02.035. These data include MOL files and InChiKeys of the most important compounds described in this article.

References

[1] H. Wisplinghoff, T. Bischoff, S.M. Tallent, H. Seifert, R.P. Wenzel, M.B. Edmond, Nosocomial bloodstream infections in US hospitals: analysis of 24,179 cases from a prospective nationwide surveillance study, Clin. Infect. Dis. 39 (2004) 309–317.

[2] J. Perlroth, B. Choi, B. Spellberg, Nosocomial fungal infections: epidemiology, diagnosis, and treatment, Med. Mycol. 45 (4) (2007) 321–346, http://dx.doi.org/10.1080/13693780701218689.

[3] J.D. Sobel, R.A. Akins, The role of resistance in *Candida* infections; Epidemiology and treatment fungal drug resistance-Clinical, in: D. Mayers (Ed.), Antimicrobial Drug Resistance, vol. 2, Clinical and epidemiological aspects, Humana Press, New York, 2009, pp. 931–951.

[4] U. Binder, C. Lass-Floerl, Epidemiology of invasive fungal infections in the Mediterranean area, Medit. J. Hemat. Infect. Dis. 3 (1) (2011) e20110016. http://dx.doi.org/10.4084/mjhid.2011.016.

[5] M.A. Pfaller, D.J. Diekema, Epidemiology of invasive mycoses in North America, Crit. Rev. Microbiol. 36 (1) (2010) 1–53.

[6] M.A. Pfaller, S.A. Messer, G.J. Moet, R.N. Jones, M. Castanheira, Candida bloodstream infections: comparison of species distribution and resistance to echinocandin and azole antifungal agents in intensive care unit (ICU) and non-ICU settings in the SENTRY Antimicrobial Surveillance Program (2008-2009), Int. J. Antimicrob. Agents 38 (1) (2011) 65–69.

[7] S. Silva, M. Negri, M. Henriques, R. Oliveira, D.W. Williams, J. Azeredo, *Candida glabrata, Candida parapsilosis* and *Candida tropicalis*: biology, epidemiology, pathogenicity and antifungal resistance, FEMS Microbiol. Rev. 36 (2) (2012) 288–305.

[8] M.A. Pfaller, M. Castanheira, S.R. Lockhart, A.M. Ahlquist, S.A. Messer, R.N. Jones, Frequency of decreased susceptibility and resistance to echinocandins among fluconazole-resistant bloodstream isolates of *Candida glabrata*, J. Clin. Microbiol. 50 (4) (2012) 1199–1203.

[9] F.C. Odds, A.J. Brown, N.A. Gow, Antifungal agents: mechanism of action, Trends Microbiol. 11 (6) (2003) 272–279.

[10] P.R. Balding, C.S. Porro, K.J. McLean, M.J. Sutcliffe, J.D. Maréchal, A.W. Munro, S.P. de Visser, How do azoles inhibit cytochrome P450 enzymes? A density functional study, J. Phys. Chem. A 112 (50) (2008) 12911–12918.

[11] J.-P. Vermitsky, T.D. Edlind, Azole resistance in *Candida glabrata*: coordinate upregulation of multidrug transporters and evidence for a Pdr1-like transcription factor, Antimicrob. Agents Chemother. 48 (10) (2004) 3773–3781.

[12] D.C. Lamb, D.E. Kelly, W.H. Schunck, A.Z. Shyadehi, M. Akhtar, D.J. Lowe, B.C. Baldwin, S.L. Kelly, The mutation T315A in *Candida albicans* sterol 14alpha-demethylase causes reduced enzyme activity and fluconazole resistance through reduced affinity, J. Biol. Chem. 272 (9) (1997) 5682–5688.

[13] K. Toté, T. Horemans, D.V. Berghe, L. Maes, P. Cos, Inhibitory effect of biocides on the viable masses and matrices of *Staphylococcus aureus* and *Pseudomonas aeruginosa* biofilms, Appl. Environ. Microbiol. 76 (10) (2010) 3135–3142.

[14] M.S.A. Khan, I. Ahmad, S.S. Cameotra, F. Botha, Sub-MICs of *Carum copticum* and *Thymus vulgaris* influence virulence factors and biofilm formation in *Candida* spp. BMC Complement, Altern. Med. 14 (2014) 337, http://dx.doi.org/10.1186/1472-6882-14-337.

[15] A. Karakurt, M. Özalp, Ş. Işık, J.P. Stables, S. Dalkara, Synthesis, anticonvulsant and antimicrobial activities of some new 2-acetylnaphthalene derivatives, Bioorg. Med. Chem. 18 (2010) 2902–2911.

[16] A. Karakurt, S. Dalkara, M. Özalp, S. Özbey, E. Kendi, J.P. Stables, Synthesis of some 1-(2-naphthyl)-2-(imidazole-1-yl)ethanone oxime and oxime ether derivatives and their anticonvulsant and antimicrobial activities, Eur. J. Med. Chem. 36 (2001) 421–433.

[17] D. De Vita, L. Scipione, S. Tortorella, P. Mellini, B. Di Rienzo, G. Simonetti, F.D. D'Auria, S. Panella, R. Cirilli, R. Di Santo, A.T. Palamara, Synthesis and antifungal activity of a new series of 2-(1*H*-imidazol-1-yl)-1-phenylethanol derivatives, Eur. J. Med. Chem. 49 (2012) 334–342.

[18] F. Moraca, D. De Vita, F. Pandolfi, R. Di Santo, R. Costi, R. Cirilli, F.D. D'Auria, S. Panella, A.T. Palamara, G. Simonetti, M. Botta, L. Scipione, Synthesis, biological evaluation and structure-activity correlation study of a series of imidazol-based compounds as *Candida albicans* inhibitors, Eur. J. Med. Chem. 83 (2014) 665–673.

[19] W. Steglich, G. Höfle, N,N-Dimethyl-4-pyridinamine, a very effective acylation catalyst, Angew. Chem. Int. Ed. 12 (8) (1969) 981–983.

[20] W. Steglich, G. Höfle, 4-Dialkylaminopyridines as acylation catalysts, 4th Communication, Synthesis 11 (1972) 619–621.

[21] B. Neises, W. Steglich, Simple method for the esterification of carboxylic acids, Angew. Chem. Int. Ed. 17 (1978) 522–524.

[22] B. Neises, W. Steglich, Esterification of carboxylic acids with dicyclohexylcarbodiimide/4-dimethylaminopyridine: tert-butyl ethyl fumarate, Org. Synth. 63 (1985) 183–185.

[23] G. Cooper, W.J. Irwin, 1-Styrylimidazoles, J. Chem. Soc. Perkin Trans. 1 (1976) 545–549.

[24] D.S. Goldfarb, Method using lifespan-altering compounds for altering the lifespan of eukaryotic organisms, and screening for such compounds, U.S. Pat. Appl. Publ. (2009). US 2009163545.

[25] C. Sheng, W. Wang, X. Che, G. Dong, S. Wang, H. Ji, Z. Miao, J. Yao, W. Zhang, Improved model of lanosterol 14α-demethylase by ligand-supported homology modeling: validation by virtual screening and azole optimization, Chem. Med. Chem. 5 (2010) 390–397.

[26] P. Vandeputte, S. Ferrari, A.T. Coste, Antifungal resistance and new strategies to control fungal infections, Int. J. Microbiol. 2012 (2012). Article ID 713687, http://dx.doi.org/10.1155/2012/713687.

[27] S. Perea, T.F. Patterson, Antifungal resistance in pathogenic fungi, Clin. Infect. Dis. 35 (9) (2002) 1073–1080.

[28] J.E. Nett, Future directions for anti-biofilm therapeutics targeting Candida, Expert Rev. Anti Infect. Ther. 12 (3) (2014) 375–382.

[29] J.C.O. Sardi, L. Scorzoni, T. Bernardi, A.M. Fusco-Almeida, M.J.S. Mendes Giannini, Antibiofilm activity *Candida* species: current epidemiology, pathogenicity, biofilm formation, natural antifungal products and new therapeutic options, J. Med. Microbiol. 62 (2013) 10–24.

[30] S.F. Altschul, W. Gish, W. Miller, E.W. Myers, D.J. Lipman, Basic local alignment search tool, J. Mol. Biol. 215 (1990) 403–410.

[31] B.C. Monk, T.M. Tomasiak, M.V. Keniya, F.U. Huschmann, J.D. Tyndall, J.D. O'Connell 3rd, R.D. Cannon, J.G. McDonald, A. Rodriguez, J.S. Finer-Moore, R.M. Stroud, Architecture of a single membrane spanning cytochrome P450 suggests constraints that orient the catalytic domain relative to a bilayer, Proc. Natl. Acad. Sci. U S A 111 (10) (2014) 3865–3870.

[32] R.A. Laskowski, M.W. MacArthur, D.S. Moss, J.M. Thornton, PROCHECK - a program to check the stereochemical quality of protein structures, J. App. Cryst. 26 (1993) 283–291.

[33] A. Šali, T.L. Blundell, Comparative protein modeling by satisfaction of spatial restraints, J. Mol. Biol. 234 (1993) 779–815.

[34] M.A. Lomize, I.D. Pogozheva, H. Joo, H.I. Mosberg, A.L. Lomize, OPM database and PPM web server: resources for positioning of proteins in membranes, Nucleic Acids Res. 40 (2012) D370–D376 (Database issue).

[35] G.I. Lepesheva, M.R. Waterman, Structural basis for conservation in the CYP51 family, Biochim. Biophys. Acta 1814 (2011) 88–93.

[36] F. Morio, C. Loge, B. Besse, C. Hennequin, P. Le Pape, Screening for amino acid substitutions in the *Candida albicans* Erg11 protein of azole-susceptible and azole-resistant clinical isolates: new substitutions and a review of the literature, Diagn. Microbiol. Infect. Dis. 66 (4) (2010) 373–384.

[37] A.G. Warrilow, C.M. Martel, J.E. Parker, N. Melo, D.C. Lamb, W.D. Nes, D.E. Kelly, S.L. Kelly, Azole binding properties of *Candida albicans* sterol 14-alpha demethylase (CaCYP51), Antimicrob. Agents Chemother. 54 (10) (2010) 4235–4245.

[38] A.G. Warrilow, J.E. Parker, D.E. Kelly, S.L. Kelly, Azole affinity of sterol 14α-demethylase (CYP51) enzymes from *Candida albicans* and *Homo sapiens*, Antimicrob. Agents Chemother. 57 (3) (2013) 1352–1360.

[39] M.V. Keniya, M. Sabherwal, R.K. Wilson, A.A. Sagatova, M.A. Woods, F.U. Huschmann, J.D.A. Tyndall, B.C. Monk, Structures of CYP51 from the pathogens *Candida glabrata* and *Candida albicans* (to be published).

[40] T. Immediata, A.R. Day, β-Napthyl derivatives of ethanolamine and N-substituted ethanolamines, J. Org. Chem. 5 (1940) 512–527.

[41] E.F. Godefroi, J. Heeres, J. Van Cutsem, P.A.J. Janssen, The preparation and antimycotic properties of derivatives of 1-phenethylimidazole, J. Med. Chem. 12 (1969) 784–791.

[42] M.L. Lopez-Rodriguez, A. Viso, S. Ortega-Gutierrez, C.J. Fowler, G. Tiger, E. de Lago, J. Fernandez-Ruiz, J.A. Ramos, Design, synthesis and biological evaluation of new endocannabinoid transporter inhibitors, Eur. J. Med. Chem. 38 (2003) 403–412.

[43] Clinical and Laboratory Standards Institute, Methods for Dilution Antimicrobial Susceptibility Tests for Bacteria that Grow Aerobically: Approved Standard, eighth ed., M07-A8. Clinical and Laboratory Standards Institute, Wayne, PA, 2008.

[44] Clinical and Laboratory Standards Institute, Reference Method for Broth Dilution Antifungal Susceptibility Testing of Yeasts: Approved Standard, third ed., M27-A3. Clinical and Laboratory Standards Institute, Wayne, PA, 2008.

[45] Innovotech Incorporated, Manufacturer's Instructions: the MBECTM Physiology&Genetics (P&G), Assay for High-throughput Antimicrobial Susceptibility Testing of Biofilms. http://www.innovotech.ca.

[46] T. Mosmann, Rapid colorimetric assay for cellular growth and survival: application to proliferation and cytotoxicity assay, J. Immunol. Methods 65 (1983) 55–63.

[47] H.M. Berman, J. Westbrook, Z. Feng, G. Gilliland, T.N. Bhat, H. Weissig, I.N. Shindyalov, P.E. Bourne, The protein data bank, Nucleic Acids Res. 28 (1) (2000) 235–242.

[48] W. Humphrey, A. Dalke, K. Schulten, VMD: visual molecular dynamics, J. Mol. Graph. 14 (1) (1996) 33–38.

[49] R.B. Best, X. Zhu, J. Shim, P.E. Lopes, J. Mittal, M. Feig, A.D. Mackerell Jr., Optimization of the additive CHARMM all-atom protein force field targeting improved sampling of the backbone φ, ψ and side-chain χ(1) and χ(2) dihedral angles, J. Chem. Theory Comput. 8 (9) (2012) 3257–3273.
[50] A.D. MacKerell Jr., M. Feig, C.L. Brooks 3rd, Improved treatment of the protein backbone in empirical force fields, J. Am. Chem. Soc. 126 (3) (2004) 698–699.
[51] A.D. MacKerell Jr., D. Bashford, M. Bellott, R.L. Dunbrack Jr., J.D. Evanseck, M.J. Field, S. Fischer, J. Gao, H. Guo, S. Ha, D. Joseph-McCarthy, L. Kuchnir, K. Kuczera, F.T.K. Lau, C. Mattos, S. Michnick, T. Ngo, D.T. Nguyen, B. Prodhom, W.E. Reiher III, B. Roux, M. Schlenkrich, J.C. Smith, R. Stote, J. Straub, M. Watanabe, J. Wiórkiewicz-Kuczera, D. Yin, M. Karplus, All-atom empirical potential for molecular modeling and dynamics studies of proteins, J. Phys. Chem. B 102 (1998) 3586–3616.
[52] W.L. Jorgensen, J. Chandrasekhar, J.D. Madura, R.W. Impey, M.L. Klein, Comparison of simple potential functions for simulating liquid water, J. Chem. Phys. 79 (1983) 926–935.
[53] K. Vanommeslaeghe, E. Hatcher, C. Acharya, S. Kundu, S. Zhong, J. Shim, E. Darian, O. Guvench, P. Lopes, I. Vorobyov, A.D. MacKerell Jr., CHARMM general force field: a force field for drug-like molecules compatible with the CHARMM all-atom additive biological force fields, J. Comput. Chem. 31 (4) (2010) 671–690.
[54] W. Yu, X. He, K. Vanommeslaeghe, A.D. MacKerell Jr., Extension of the CHARMM general Force field to sulfonyl-containing compounds and its utility in biomolecular simulations, J. Comput. Chem. 33 (2012) 2451–2468.
[55] T. Darden, D. York, L. Pedersen, Particle mesh Ewald: an N log (N) method for Ewald sums in large systems, J. Chem. Phys. 98 (12) (1993) 10089–10092.
[56] J.C. Phillips, R. Braun, W. Wang, J. Gumbart, E. Tajkhorshid, E. Villa, C. Chipot, R.D. Skeel, L. Kalé, K. Schulten, Scalable molecular dynamics with NAMD, J. Comput. Chem. 26 (16) (2005) 1781–1802.
[57] J.L. Banks, H.S. Beard, Y. Cao, A.E. Cho, W. Damm, R. Farid, A.K. Felts, T.A. Halgren, D.T. Mainz, J.R. Maple, R. Murphy, D.M. Philipp, M.P. Repasky, L.Y. Zhang, B.J. Berne, R.A. Friesner, E. Gallicchio, R.M. Levy, Integrated modeling program, applied chemical theory (IMPACT), J. Comput. Chem. 26 (16) (2005) 1752–1780.
[58] G.M. Sastry, M. Adzhigirey, T. Day, R. Annabhimoju, W. Sherman, Protein and ligand preparation: parameters, protocols, and influence on virtual screening enrichments, J. Comput. Aid. Mol. Des. 27 (3) (2013) 221–234.
[59] J.R. Greenwood, D. Calkins, A.P. Sullivan, J.C. Shelley, Towards the comprehensive, rapid, and accurate prediction of the favorable tautomeric states of drug-like molecules in aqueous solution, J. Comput. Aided Mol. Des. 24 (2010) 591–604.
[60] J.C. Shelley, A. Cholleti, L. Frye, J.R. Greenwood, M.R. Timlin, M. Uchimaya, Epik: a software program for pKa prediction and protonation state generation for drug-like molecules, J. Comp. Aided Mol. Des. 21 (2007) 681–691.
[61] G.M. Morris, R. Huey, W. Lindstrom, M.F. Sanner, R.K. Belew, D.S. Goodsell, A.J. Olson, Autodock4 and AutoDockTools4: automated docking with selective receptor flexibility, J. Comput. Chem. 30 (16) (2009) 2785–2791.